VIRGINIA POLYTECHNIC INSTITUTE
AND STATE UNIVERSITY LIBRARIES

Virginia Water Resources Research Center Bulletin 111

Modeling Sediment Movement in the Turbidity Maximum of an Estuary

Albert Kuo
Maynard Nichols
James Lewis

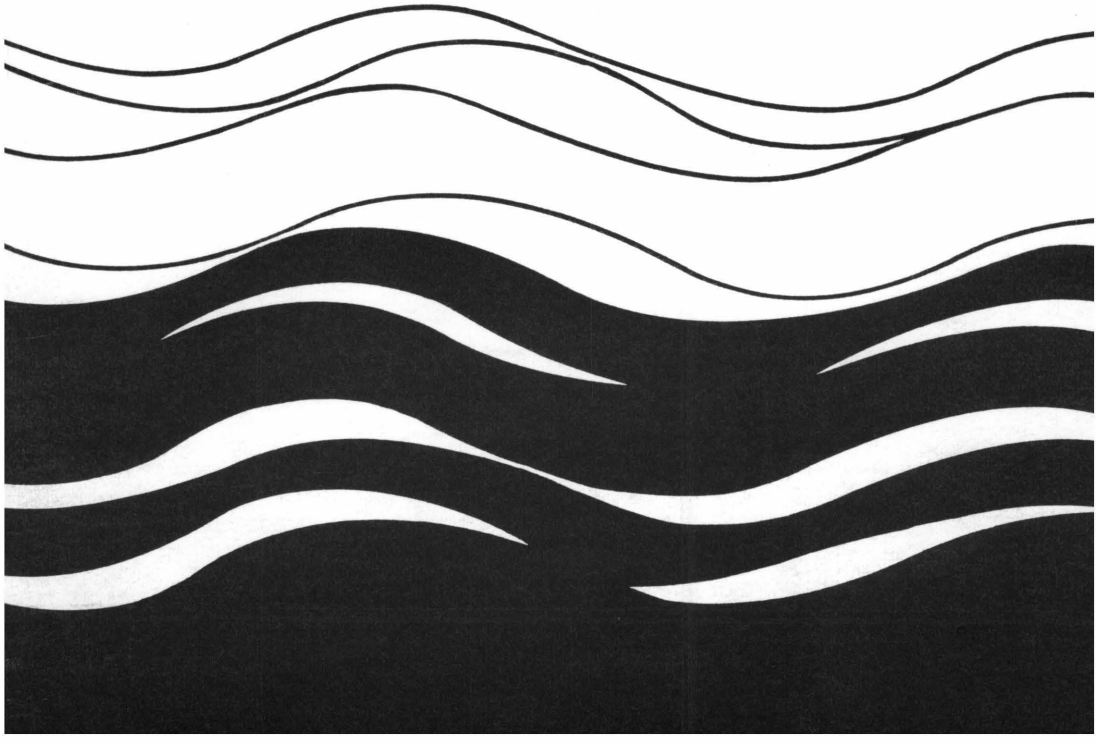

Bulletin 111
June 1978

Modeling Sediment Movement in the Turbidity Maximum of an Estuary

Albert Kuo
Maynard Nichols
James Lewis

Virginia Institute of Marine Science
Gloucester Point, Virginia 23062

The work upon which this report is based was supported in part by funds provided by the United States Department of the Interior, Office of Water Research and Technology, as authorized by the Water Resources Research Act of 1964 (P.L. 88-379).

OWRT Project B-077-VA
VPI-VWRRC-BULL 111

A publication of
Virginia Water Resources Research Center
Virginia Polytechnic Institute and State University
Blacksburg, Virginia 24060

TD
201
V57
no. 111
c. 2

Additional copies of this publication,
while the supply lasts, may be obtained from
the Virginia Water Resources Research Center.
Single copies are provided free to persons
and organizations within Virginia. For those
out-of-state, the charge is $4 per copy
if payment accompanies the order, or $6
per copy if billing is to follow.

TABLE OF CONTENTS

LIST OF FIGURES

ABSTRACT

This research developed a two-dimensional, time-dependent numerical model to simulate the movement of water and suspended sediment in the turbidity maximum of an estuary. This model is a systematic sequence of mathematical procedures derived from the mass-balance equation and the equation of motion. Lateral integration is used to obtain two-dimensional equations; these equations are integrated with depth over the height of successive layers. Finite difference equations then are written for each layer and solved numerically using prescribed boundary conditions.

The model yields values for time-varying tidal height, current speed, salinity, and suspended sediment concentration (turbidity) throughout the estuary. In turn, these variations reveal the response to tidal current fluctuations of both salinity and sediment distributions within the maximum. Residual values of each parameter are obtained by averaging respective values over a tidal cycle. By examining the time-varying and the tidal average transport at landward and seaward transects, sediment transport through the turbidity maximum may be studied in detail. Using this numerical model permits analyses of hydraulic processes that lead to suspended sediment accumulation.

Key Words: Mathematical Model, Estuaries, Sediment Transport, Turbidity Maximum

ACKNOWLEDGMENTS

Special acknowledgment is accorded the following who generously gave their time to a critical review of the manuscript: Donn G. DeCoursey, Agricultural Research Service, U.S. Department of Agriculture; and D.L. Reddell, Agricultural Engineering Department, Texas A & M University. Acknowledgment is made also to Nancy L. Chapman for editorial processing and typesetting and to Patricia A. Nickinson for lay-out composition.

INTRODUCTION

The need to improve water quality resulting from excess sediment loads and turbidity in estuaries has prompted an advanced analysis of sediment transport. Concentrations of suspended sediment in middle reaches of Virginia's James and Rappahannock Rivers are often higher than in source river water or sea water. How does the suspended sediment accumulate to form a turbidity maximum? What processes are significant in producing an "excess" sediment load and what is their relative importance? How would proposed alterations like channel deepening and river dams affect the turbidity maximum? Mathematical modeling is one approach to answering these questions.

I. Purpose of the Study

The purpose of this study is three-fold:

1. To formulate a model to simulate the distribution of suspended sediment and current velocity in an estuary and particularly, in a turbidity maximum.

2. To describe in mathematical terms the systematic motion of water and sediment, as well as the transport processes active in a maximum.

3. To determine if the processes are correctly represented and if the computational procedures are valid.

II. Relevance to Water Resources

Suspended sediment is a key determinate affecting water quality in Virginia estuaries. It is the chief cause of turbidity that degrades estuarine ecology by dampening light penetration, reducing thickness of the euphotic zone, and in turn, limiting basic productivity. Extreme turbidity threatens fish habitats by clogging gill structures and interfering with respiration. Suspended sediment that settles out, especially high loads supplied by a flood like Storm Agnes, may bury clams and oysters or impair setting sites of planktonic larvae.

Contaminants like heavy metals, insecticides such as Kepone, petroleum by-products, and some radio-nuclides are readily absorbed by silt and

clay particles. Consequently, suspended sediment enriched with contaminants is a form of pollution. When filter-feeding organisms ingest suspended sediment, they often concentrate the contaminants or recycle them as fecal pellets. When contaminated particles are transported by estuarine currents, they are subject to accumulation like natural silt particles in the turbidity maximum. Concentration factors of more than 100,000 have been observed in some estuaries [Postma, 1969]. As a result of rapid sediment accumulation and long residence time, the turbidity maximum is one of the most vulnerable zones to pollution in an estuary.

Organic detritus and nutrients, either in particulate form or adsorbed on sediment particles, also accumulate with natural sediment in the turbidity maximum. Organic-rich sediments reduce dissolved oxygen concentration and create a sag in the longitudinal oxygen distribution. This effect is compounded when oxygen production of plants is simultaneously reduced by high turbidity.

The problem of improving water quality resulting from high suspended sediment loads has become complicated in recent years by the activities of man. As noted by Meade and Trimble [1974], sediment input to estuaries often is increased by urban development and intensified land use. For example, conversion of forests to cropland in the Piedmont increases sediment yields about 10 times, while coal mining and housing developments add enormous loads, often 20 to 30 times the natural discharge. By contrast, the input is reduced by construction of dams, diversion of rivers, and control of shore erosion along banks. The problem is complicated further by channel dredging and disposal of dredge material within estuaries. Such activities that affect water quality do not operate alone but often they are additive, carrying with them a potential for cumulative effects over time. Such effects are extended throughout estuaries via the active circulation.

It is not surprising, therefore, that scientists and engineers have developed a keen interest in understanding and predicting the movement of water and sediment. Assessing impacts of proposed changes requires an advanced knowledge of environmental effects before the changes are accomplished. To this end, a computerized mathematical model based on physical principles offers one approach to gain the needed predictive capability. A predictive understanding of dynamic responses in an estuary should strengthen state and federal abilities to design guidelines for im-

proving water quality essential to better recreation and estuarine food production.

STATUS OF ESTUARINE SEDIMENT TRANSPORT MODELS

For years, researchers have developed mathematical models of waste loading, dissolved oxygen, and salinity balance, but few have attempted to model suspended sediment transport in an estuary. The current state-of-the-art began with the pioneering effort of Odd and Owen [1972]. These workers formulated a one-dimensional model to simulate the tidal flow and transport of mud in the Thames, a well-mixed estuary. Since the flow and suspended sediment concentration change with depth, mainly near the bed, flow was divided into two unequal layers. The model assumed uniform properties in each layer and a rectangular section. According to the workers, simplifications could be made without significantly affecting the accuracy of the model because of its relatively narrow and exponentially varying width, virtually constant depth, good tidal mixing, and sinusoidal curves at the mouth. Equations of motion and continuity were solved by the finite difference method, and the mass balance equations for suspended sediment were solved by the method of characteristics.

Odd and Owen used depth-averaged values in each layer, which could cause the model to distort the advective effect of the tidal currents unless corrected by a factor. The exchange of suspended matter by settling and vertical mixing between layers also requires improved numerical representation.

In another treatment of suspended sediment transport, Ariathurai [1974] formulated a two-dimensional (in horizontal plane) depth-averaged model with convection-diffusion equations of mass conservation solved by the finite element method. A source-sink term was evaluated at each time step from the previous concentration. According to Ariathurai, the model requires a specified flow field, diffusion coefficients, and laboratory sediment characteristics as determined by Krone [1962]. Since diffusion coefficients and sediment properties can be specified for each element, continuing aggregation could be accounted for by specifying the appropriate settling velocity in each element. Once verified by field observations in the Savannah, it is anticipated that the model can be used with vertical and axial dimensions in areas where lateral averaging is feasible. Greater accuracy would be attained by including depth as one of the dimensions.

Christodoulou, Leimkuhler, and Ippen [1974] presented a quasi-three-dimensional model in which the vertical distribution of sediment is com-

puted from the average concentration. The main considerations and assumptions are:

1. The velocity field is composed of net flow with a superimposed sinusoidal tidal velocity.

2. The depth of flow is constant.

3. The dispersion coefficients bear a simple relation to the shear velocity.

4. Sediment has a single vertical line source and all particles reaching the bed stick to it.

5. The vertical distribution of sediment is independent of concentration.

Because the quasi-steady state solution resulting from the assumed vertical distribution is reliable for sediment variations less than about two tidal cycles, the model is useful mainly for long-term sedimentation in a slowly varying velocity field, such as dredge spoil disposal, rather than in a rapidly varying resuspension regime of the turbidity maximum.

In upper Chesapeake Bay, Hunter [1975] attempted to develop a three-dimensional numerical model to predict the source field from the concentration field of a passive contaminant subject to advection, diffusion, and settling. The results aid in predicting the vertically-integrated source function, i.e., the flux of sediment per unit horizontal area per unit time. But as Hunter indicates, "The results do not tell us any more than we already know—that sediment enters the Bay via the Susquehanna and leaves it by the southern open boundary."

Schubel and Carter [1977] used a simple single segment model to estimate the annual mean sedimentation rate in the Chesapeake Bay. Additionally, they used the model to estimate the net suspended sediment exchange rates among the Bay, its tributaries, and adjacent ocean. Net advection follows the salt balance through upper and lower estuarine layers. The flux of water is then substituted in an equation expressing the conservation of suspended sediment. The model results indicate a net movement of sediment into the Bay from the ocean while tributary estuaries, like the Rappahannock, serve as sinks for suspended sediment from the Bay.

A three-dimensional, time-dependent model is necessary to fully simulate estuarine flow and suspended sediment processes which are three-dimensional in nature. Leendertse, Alexander, and Liu [1973] and also Caponi [1974 and 1976] developed three-dimensional mathematical models for flow in estuaries, bays, and coastal seas. The application of these models is a formidable task due to the large computer storage capacity, long computation time, and resulting expense. None of these three-dimensional models has been calibrated or verified, partly because of the large expenditure of effort required to collect the data. Until sedimentary processes are better known and the three-dimensional models can be verified, a simple two-dimensional, time-dependent model including the depth dimension provides the best tool.

Although several models are available for suspended sediment transport behavior in simple estuarine situations, application to processes active in the turbidity maximum is relatively new. Two models currently are being developed by researchers—D. O'Connor, Manhattan College [personal communication, 1977]; and J. Festa, National Oceanic and Atmospheric Association [personal communication, 1976]—but the utility of these models remains to be demonstrated. For a model to be useful in a variety of estuaries, it must be based on fundamental laws of motion, continuity, and mass balance. Its reliability must be tested through calibration and verification based on field observations and transport behavior, but must not be too expensive.

ESTUARINE SUSPENDED SEDIMENT

I. Sediment Characteristics

Suspended sediment in the turbidity maximum of the Rappahannock and the James mainly consists of silt and clay particles finer than 12μ m. Generally, the particle size varies narrowly with distance seaward from the river into saline reaches. Particles are composed mainly of quartz and the clay minerals illite and chlorite mixed with small percentages of organic detritus (<15 percent), plankton, and skeletal material like diatom frustules. Floccules are scarce but a great amount of suspended sediment is weakly bound into composite particles or agglomerates as well as fecal pellets. Such particles are larger than individual particles and thus tend to settle faster in a given flow field because of their relatively fast settling velocities. Bottom sediments, which are a proximate source of much suspended sediment in the turbidity maximum, mainly consist of silt and clay. Particle size is very small, less than 10μ m mean size, and it varies within narrow limits longitudinally through the reach of the maximum, from 3.0 to 6.5μ m. However, farther landward and seaward of the maximum, particles generally are coarser than in the maximum itself.

Suspended sediment in the turbidity maximum is mainly derived from the drainage basin. The average yearly influx of the Rappahannock at Fredericksburg amounts to an estimated 0.25 megatons. Erosion of shores and banks adds approximately 0.11 megatons of silt and clay yearly [Byrne and Anderson, 1977], while skeletal material and organic production add about 0.10 megatons yearly. An unknown fraction is supplied through the mouth via the lower estuarine layer from Chesapeake Bay. More than 70 percent of each year's supply of river-borne sediment is delivered during short pulses of freshet and flood. The bulk of this load is deposited in the zone of the turbidity maximum where rates reach 17 mm per year. Less than 10 percent of the river-borne load escapes from the Rappahannock Estuary.

II. Sediment Transport Processes

The movement of fine sediment in the Rappahannock is basically a cycle of three processes: erosion, transportation in suspension, and deposition. Each process is a transient affair. The transport load not only changes with time but also with distance seaward and with depth throughout the

turbidity maximum. Changes are produced by turbulence, tidal currents, meteorological forces, river discharge, and density currents. The rate and routes of sediment movement are complex and partly depend on sediment properties which are not fully known. Therefore, recourse has to be made to empirical expressions (e.g., Harrison and Owen, [1971]), or quantitative relationships based on laboratory studies (e.g., Krone, [1962 and 1963]). Consequently, modeling sediment transport requires calibration and verification of the expressions over a range of conditions.

The most obvious movement of water and sediment in the Rappahannock is produced by tidal currents. Concentrations of suspended sediment at any given point increase and decrease as current speed changes with time from nearly 0 at slack water to about 0.5 m/sec at maximum current and then to nearly 0 at the following slack water. Such changes not only take place at a given point but throughout the water column *(Figure 1)*. Since concentrations increase more rapidly during early flood than they decrease during late flood, an asymmetrical time distribution is displayed. Settling time is longer around the slack before ebb—a time when the maximum is more depleted—than around the slack before the flood. When these asymmetrical distributions are obtained over many tidal cycles, the net result should produce a net landward shift of sediment. However, the repetitive tidal resuspension of sediment from the bottom not only depends on the tidal current speed but also on properties of the bottom sediment.

When the tidal current exerts a shear stress on the bed which exceeds a certain value called the "critical shear stress," erosion of bed particles occurs. At high levels of shear stress—when the current overpowers the shear strength of the cohesive bed sediment—mass erosion and suspension occur. In the Rappahannock, clouds of bed sediment "burst" off the bottom when currents exceed about 18 cm/sec.

Sediment removed from the bed is transported in suspension as long as turbulence and upward diffusion exceed downward settling. In general, concentrations increase from the surface toward the bottom, but they are not great enough to create flocs with settling rates higher than dispersed suspended sediment.

Deposition of suspended sediment occurs when the shear stress on the bed falls below a certain value called the "limiting shear stress for deposition." Depending on the cohesive character of the bed and its resistance

to shear stress, this value may be the same or less than the critical shear stress for erosion. Net deposition on the bed is the difference between the total quantities of deposition and erosion over many tidal cycles.

Very fine-grained sediment that remains in suspension for long periods is transported through upper and lower estuarine layers by two-way density currents. Despite the back and forth movement of tidal currents, river water flows seaward through freshened parts of the upper estuary both near the surface and near the bottom *(Figure 2)*. Farther seaward, river water spreads out over salty water. Although tidal currents mix the salty water with overlying freshened water, distinctive layers persist.When suspended sediment settles out from the upper layer into the lower layer, it is transported landward by density currents to a zone where landward and seaward currents meet. Because net current speed is so small in this zone, called a "null zone" *(Figure 2)*, suspended sediment supplied either from the river or from the lower layer resides in the zone for a long time. Sediment that is too heavy to be mixed upward and carried back seaward in the upper layer is trapped. Entrapment goes on as long as there is a supply of sediment from the river or the lower estuarine layer.

THE TURBIDITY MAXIMUM

I. Time and Space Variations

The turbidity maximum occupies a large zone, 20 to 30 km long, where suspended sediment concentrations are greater than in river water or in estuarine water. In Virginia estuaries, the maximum is located near the inner limit of salty water *(Figure 3)*. The concentrations are higher near the bottom, where they range from 100 to 300 mg/l, than near the surface, where they range from 25 to 60 mg/l. Such concentrations attain highest values 10 to 20 cm above the bottom. Thus, there is a downward gradient of increasing sediment concentration toward the bottom.

The turbidity maximum is not a permanent feature but it continuously changes its load and shifts position in response to river inflow. During a river flood like Agnes, the maximum acquires high concentrations and is located in a narrow null zone of the lower estuary. By contrast, as river inflow diminishes, the maximum loses its load and shifts landward with landward migration of the salt intrusion head and the null zone.

The load of sediment in the maximum also varies with the strength of tidal currents as they change from neap to spring tide range over a fortnightly cycle. With increasing tidal range, current velocities increase sediment resuspension from the bottom and augment the load in the maximum 10 to 50 fold. During decreasing tidal range, the average concentrations decrease, often attaining a minimum during neap tide range. Despite the tidal changes, sediment loads in the maximum are mainly affected by the river-borne sediment influx.

II. Data Input

Observations of the turbidity maximum in the Rappahannock Estuary consist of spatial and time-series measurements of current velocity, salinity, and suspended sediment concentrations. Forty-two longitudinal transects were run between December 1970 and August 1972 at various stages of the tide and at different levels of river inflow, including increased levels resulting from Storm Agnes. In addition, four anchor stations were occupied simultaneously along the length of the maximum at three levels of river inflow: 141 m^3/sec, 53 m^3/sec, and 23 m^3/sec at Fredericksburg. Measurements were made continuously at three to four depth intervals for periods of eight to 26 tidal cycles in April 1970 and in April and May

1971. Observational details and analytical procedures are given in Nichols and Thompson [1973]. The results reveal the dynamic behavior of the turbidity maximum induced by estuarine density currents and by tidal currents.

III. The Physical System—Rappahannock Estuary

The Rappahannock Estuary offers several advantages for modeling. Its configuration is relatively straight and its bottom geometry is simple. There is a single axial channel which deepens irregularly with distance seaward from 5 m at Tappahannock to 24 m at the mouth. Shoals, averaging 2 m to 3 m deep, border the main channel. The estuary is largely free of extensive pollution, and sedimentation is unaffected by major dams and extensive channel dredging. Because the estuary is 175 km long (including the tidal portion of the river) and narrow (less than 8 km), lateral variations of flow and sediment concentration are small relative to the longitudinal variations. This feature allows a two-dimensional (vertical and longitudinal) analysis.

Hydrodynamic conditions in the estuary are relatively mild. The tide range is 51 cm at the head and 33 cm at the mouth. Corresponding mean tidal velocities are 65 and 32 cm/sec. At average conditions of tide and river inflow estuary water is partly mixed. Fresh and salty water mix over a broad transition zone and stratification is weak.

TIDAL-TIME MODEL

I. Approach

The tidal-time model consists of a systematic sequence of numerical procedures designed to describe and to simulate the main movement of water and suspended sediment in an estuary. The chief parameters of numerical computation are tidal height, current, salinity, and suspended sediment concentration in response to the basic external forces: tide wave propagation, river inflow, and river-borne sediment influx. Inasmuch as the forces and parameters are continuously interacting and rapidly changing with time, the model is time-dependent.

Since Virginia estuaries are long and narrow and suspended sediment concentrations in the turbidity maximum change significantly with distance seaward and with depth, the model is two-dimensional. It is assumed that all properties are uniformally distributed laterally across the estuary at their respective average values.

To calculate the movement of water and suspended sediment distribution, the time-dependent, three-dimensional equations of motion and the equation of mass balance are first integrated laterally to obtain two-dimensional equations. Next, the two-dimensional equations are integrated with depth over the height of successive layers, and the resulting equations for each layer are written in explicit finite difference forms. The finite difference equations are then solved numerically with prescribed initial and boundary conditions.

The numerical computation yields the time-varying tidal height, current, salinity, and suspended sediment concentration distribution throughout the estuary. Thus, these time variations display the response of salinity and sediment distributions to tidal current fluctuations such as the resuspension of sediment particles during increasing flood or ebb current strength as well as deposition during slack current periods. Sediment flux at any transect may be calculated by multiplying the horizontal velocity with sediment concentration and integrating over the cross-section. Residual values can be obtained for each parameter by averaging the respective parameter over a complete tidal cycle. The average sediment concentration field defines the turbidity maximum if the hydrographic conditions lead to development of a maximum. The transport through the zone of

turbidity maximum then may be studied in detail by examining the time-varying and tidal average transport at its landward and seaward transects.

II. Basic Equations

Odd and Owen [1972] state, "The ability of a mathematical model to simulate complex tidal processes such as mud transport, depends on the degree to which the various physical processes can be described in mathematical terms and on a knowledge of the laws involved." The terms used for describing the motion of suspended sediment generally are included within two partial differential equations: the equation of motion and that for the conservation of mass. These equations are generally flexible enough for a variety of integration schemes and boundary conditions.

The basic equations used to represent and calculate the flow field and suspended sediment concentration field for this model are:

$$\frac{\partial u}{\partial t} + \frac{\partial (u^2)}{\partial x} + \frac{\partial (uv)}{\partial y} + \frac{\partial (uw)}{\partial z} =$$

$$- \frac{1}{\rho} \frac{\partial P}{\partial x} + \frac{\partial}{\partial x} \left(e_x \frac{\partial u}{\partial x}\right) + \frac{\partial}{\partial y} \left(e_y \frac{\partial u}{\partial y}\right) + \frac{\partial}{\partial z} \left(e_x \frac{\partial u}{\partial z}\right) \qquad (1)$$

$$- g = \frac{1}{\rho} \frac{\partial P}{\partial z} \qquad (2)$$

$$\frac{\partial u}{\partial x} + \frac{\partial v}{\partial y} + \frac{\partial w}{\partial z} = 0 \qquad (3)$$

$$\frac{\partial s}{\partial t} + \frac{\partial (us)}{\partial x} + \frac{\partial (vs)}{\partial y} + \frac{\partial (ws)}{\partial z} =$$

$$\frac{\partial}{\partial x} \left(\varepsilon_x \frac{\partial s}{\partial x}\right) + \frac{\partial}{\partial y} \left(\varepsilon_y \frac{\partial s}{\partial y}\right) + \frac{\partial}{\partial z} \left(\varepsilon_z \frac{\partial s}{\partial z}\right) \qquad (4)$$

$$(P + P_o) \left(\frac{1}{\rho} - \frac{1}{\rho_o}\right) = \lambda \qquad (5)$$

$$\frac{\partial c}{\partial t} + \frac{\partial (uc)}{\partial x} + \frac{\partial (vc)}{\partial y} + \frac{\partial ((w-V)c)}{\partial z} =$$

$$\frac{\partial}{\partial x} \left(\varepsilon_x \frac{\partial c}{\partial x}\right) + \frac{\partial}{\partial y} \left(\varepsilon_y \frac{\partial c}{\partial y}\right) + \frac{\partial}{\partial z} \left(\varepsilon_z \frac{\partial c}{\partial z}\right) - d + r \qquad (6)$$

where:

u, v, w	=	velocity components in the x, y, and z directions, respectively;
t	=	time;
P	=	pressure;
ρ	=	density of water;
e_x, e_y, e_z	=	turbulent viscosities in the x, y, and z directions, respectively;
g	=	gravitational acceleration;
s	=	salinity;
$\epsilon_x, \epsilon_y, \epsilon_z$	=	turbulent diffusion coefficients in the x, y, and z directions, respectively;
P_o, ρ_o, λ	=	empirical functions of temperature and salinity;
c	=	suspended sediment concentration;
V	=	sediment settling velocity;
d	=	sediment deposition rate;
r	=	sediment resuspension rate;

and the coordinate system is as follows:

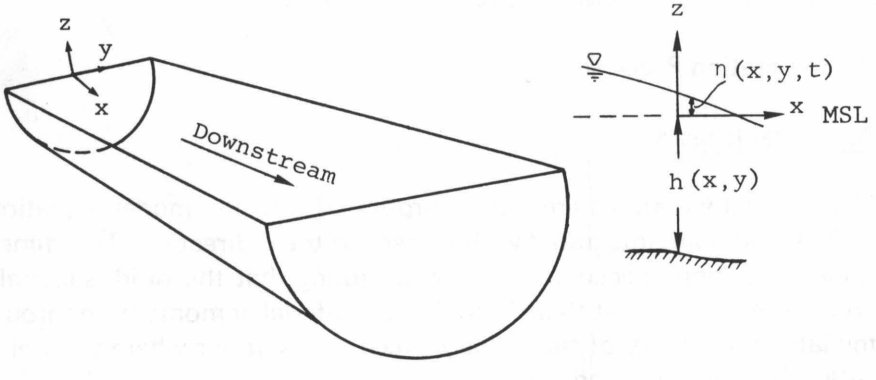

Equation 1 is the equation of motion for an incompressible but non-homogeneous fluid and represents the longitudinal momentum of estuarine water. For the equation of motion in the vertical direction, gravity is assumed to be the dominant force which leads to the hydrostatic equation 2. Equation 3 is the continuity equation for an incompressible fluid, and equation 4 is the mass-balance equation for salts. Equation 5 is an empirically derived "equation of state" [Eckart, 1958] relating water density

with salinity, temperature, and pressure. The equation of state may be simplified since the effect of pressure on density is negligible for the water depths (i.e., $P \cong 0$). This simplification gives:

$$\rho = \frac{P_o}{\lambda + \frac{P_o}{\rho_o}} \tag{7}$$

where:

$$\lambda = 1779.5 + 11.25T - .0745T^2 - (3.80 + .017T) \cdot s$$

$$\rho_o = 1.4326$$

$$P_o = 5890 + 38T - .375T^2 + 3s$$

where:

ρ = density in gm/cm^3;
T = temperature in Celsius;
s = salinity in parts per thousand.

Equation 6 is the mass-balance equation for suspended sediment, with resuspension and deposition as source and sink.

III. Integration Processes

A. Lateral Integration

Since lateral variations are not incorporated into the model, equations 1, 3, 4, and 6 are integrated with respect to the y direction. This dimensional reduction is accomplished by assuming that the fluid is laterally homogeneous and that there is no flux of material or momentum through the lateral boundary of the estuary except at locations where tributaries enter. The equations reduce to:

$$\frac{\partial}{\partial t}(uB) + \frac{\partial}{\partial x}(uBu) + \frac{\partial}{\partial z}(wBu) = -\frac{B}{\rho}\frac{\partial P}{\partial x} + \frac{\partial}{\partial x}\left(e_x B\frac{\partial u}{\partial x}\right) + \frac{\partial}{\partial z}\left(e_z B\frac{\partial u}{\partial z}\right) + qu_t \tag{8}$$

$$\frac{\partial}{\partial x}(uB) + \frac{\partial}{\partial z}(wB) = q \tag{9}$$

$$\frac{\partial}{\partial t}(Bs) + \frac{\partial}{\partial x}(uBs) + \frac{\partial}{\partial z}(wBs) =$$

$$\frac{\partial}{\partial x}\left(\varepsilon_x B\frac{\partial s}{\partial x}\right) + \frac{\partial}{\partial z}\left(\varepsilon_z B\frac{\partial s}{\partial z}\right) + q\, s_t \qquad (10)$$

$$\frac{\partial}{\partial t}(Bc) + \frac{\partial}{\partial x}(uBc) + \frac{\partial}{\partial z}((w-V)\,Bc) =$$

$$\frac{\partial}{\partial x}\left(\varepsilon_x B\frac{\partial c}{\partial x}\right) + \frac{\partial}{\partial z}\left(\varepsilon_z B\frac{\partial c}{\partial z}\right) - Bd + Br + qc_t \qquad (11)$$

where:

B = width of estuary;
q = tributary inflow (or outflow) through unit area of x-z plane;
u_t, s_t
c_t = longitudinal velocity, salinity, and sediment concentrations of tributary flow, respectively.

In case the estuary is only approximately laterally homogeneous, the dependent variables (u, s, and c of the above equations) should be interpreted as lateral average values and the turbulent viscosities and diffusion coefficient should take account of the lateral shear effect[Fisher,1967].

To obtain the time-varying solution of the longitudinal and vertical velocity field, equation 8 must be solved with the continuity equation (equation 9) and the salt mass-balance equation (equation 10). The equation of state is used in order to evaluate the pressure term in the longitudinal equation of motion. With the velocity field solved, it may be substituted into equation 11 to solve for the time-varying concentration field of suspended sediment.

B. Vertical Integration

Since variables in estuaries can change rapidly over a short vertical distance, they require a grid size that is much smaller in the vertical direction than in the longitudinal direction. To accomplish this, the fluid motion will be considered in horizontal slices with an exchange of mass and momentum between these slices. The geometry of the grid system used in the model and the location of variables within the grid are shown in *Figure 4,* with η representing the surface elevation with respect to mean sea level. To determine the spatial location of a variable, a longitudinal and a vertical subscript are used.

Integration over the height of the *k*th layer can be performed by assuming that all variables are practically constant through the depth of any layer and that the fluxes of momentum and mass normal to the bottom of the channel and to the surface are 0. One can employ Liebnitz's rule and obtain the following equations:

$$\frac{\partial \eta}{\partial t} = \frac{1}{B_1} \left(w_b B_b - \frac{\partial}{\partial x} (u_1 B_1 h_1) + q_1 h_1 \right) \tag{12}$$

$$w_T = \frac{1}{B_T} \left(w_b B_b - \frac{\partial}{\partial x} (u_k B_k h_k) + q_k h_k \right) \tag{13}$$

$$\begin{aligned} &\frac{\partial}{\partial t} (u_k B_k h_k) + \frac{\partial}{\partial x} (u_k B_k h_k u_k) + w_T u_T B_T - w_b u_b B_b \\ &\quad = - \frac{B_k h_k}{\rho_k} \left(\frac{\partial P}{\partial x}\right)_k + \frac{\partial}{\partial x} \left(e_{x_k} B_k h_k \left(\frac{\partial u}{\partial x}\right)_k\right) \\ &\quad + \tau_T - \tau_b + q_k u_t h_k \end{aligned} \tag{14}$$

$$\begin{aligned} &\frac{\partial}{\partial t} (s_k B_k h_k) + \frac{\partial}{\partial x} (u_k B_k h_k s_k) + w_T s_T B_T - w_b s_b B_b \\ &\quad = \frac{\partial}{\partial x} \left(\varepsilon_x h \frac{\partial s}{\partial x}\right)_k + \left(\varepsilon_z B \frac{\partial s}{\partial z}\right)_T - \left(\varepsilon_z B \frac{\partial s}{\partial z}\right)_b + q_k s_t h_k \end{aligned} \tag{15}$$

$$\begin{aligned} &\frac{\partial}{\partial t} (c_k B_k h_k) + \frac{\partial}{\partial x} (u_k B_k h_k c_k) + (w_T - V) c_T B_T - (w_b - V) c_b B_b \\ &\quad = \frac{\partial}{\partial x} \left(\varepsilon_x h B \frac{\partial c}{\partial x}\right)_k + \left(\varepsilon_z B \frac{\partial c}{\partial z}\right)_T - \left(\varepsilon_z B \frac{\partial c}{\partial z}\right)_b - Bd + Br \\ &\quad + q_k c_t h_k \end{aligned} \tag{16}$$

where:

B_k, u_k, h_k, q_k = width, longitudinal velocity, height, and tributary inflow for the *k*th layer, respectively;

u_b, w_b, B_b = longitudinal velocity, vertical velocity, and estuary width, respectively, at the bottom of a layer;

$u_T, w_T,$
B_T = longitudinal velocity, vertical velocity, and estuary width, respectively, at the top of a layer;

$\tau_T = (e_z B \frac{\partial u}{\partial z})_T$ and $\tau_b = (e_z B \frac{\partial u}{\partial z})_b$ = interfacial shear stresses.

Equation 12 is the continuity equation for the top layer, whereas equation 13 is the continuity equation for all other layers. Equation 14 is the longitudinal equation of motion, and equations 15 and 16 are the mass balance equations for salt and suspended sediment. Further development of the pressure term $\frac{B_k h_k}{\rho_k} (\frac{\partial P}{\partial x})_k$ is given in the following section.

C. The Pressure Term in the Equation of Motion

From the hydrostatic equation (equation 2), $\Delta P = -\rho g \Delta z$. An approximation using this equation and the layers in the model is:

$$P_{k-1} - P_k = -g(\rho_{k-1}\frac{h_{k-1}}{2} + \rho_k \frac{h_k}{2}) \tag{17}$$

This gives:

$$(\frac{\partial P}{\partial x})_k = (\frac{\partial P}{\partial x})_{k-1} + \frac{gh_{k-1}}{2}\frac{\partial \rho_{k-1}}{\partial x} + \frac{gh_k}{2}\frac{\partial \rho_k}{\partial x} \tag{18}$$

The term of interest in the equation of motion is the integral from the bottom to the top of a layer of $\frac{B}{\rho}\frac{\partial P}{\partial x}$, or $\frac{B_k}{\rho_k} h_k (\frac{\partial P}{\partial x})_k$, where $(\frac{\partial P}{\partial x})_k$ is the pressure gradient averaged over the *k*th layer and given in equation 18. Therefore, if $(\frac{\partial P}{\partial x})_1$ can be calculated, all other $(\frac{\partial P}{\partial x})_k$'s can be calculated. For the top layer:

$$\frac{\partial P}{\partial x} = \frac{\partial}{\partial x}\{g\rho_1(\eta - z)\} ,$$

from the hydrostatic equation. From this, it can be shown that:

$$\int_{-h_1}^{\eta} \frac{B}{\rho}\frac{\partial P}{\partial x}\, dz = \frac{B_1(h_1+\eta)}{\rho_1} \cdot (\frac{g}{2}(h_1+\eta)\cdot\frac{\partial \rho_1}{\partial x} + g\rho_1 \frac{\partial \eta}{\partial x}) \tag{19}$$

Thus, for the top layer:

$$\left(\frac{\partial P}{\partial x}\right)_1 = \frac{g}{2}(h_1 + \eta) \cdot \frac{\partial \rho_1}{\partial x} + g\rho_1 \frac{\partial \eta}{\partial x} \tag{20}$$

This allows the pressure term in the equation of motion to be calculated for each layer.

IV. Boundary Conditions at the Surface and Bottom

A. Velocity Components

As shown in *Figure 4,* the bottom boundary is defined through the grid point where the vertical velocity component is specified. Therefore, the vertical velocity at the bottom layer is 0, i.e., $W_b = 0$, for bottom layer. At the free surface, no velocity component needs to be specified. The vertical velocity component W_T at the top of the first layer is set implicitly to 0 to assure no flux of mass accross free surface.

B. Boundary Stresses

The wind stress and bottom friction are used in order to account for energy introduced into the estuary by wind and energy dissipated by frictional force. The formulation used for this model is the well-known quadratic law:

$$\text{wind stress} = C\,\rho_a\,W^2, \tag{21}$$

where:

C = drag coefficient (= 1.3×10^{-3});
ρ_a = air density (= 1.2×10^{-3} gm/cm^3);
W = wind speed at height of 10 m.

$$\text{bottom stress} = \rho u_b |u_b| \cdot gn^2 (h_b)^{-1/3} \tag{22}$$

where:

ρ, u_b, h_b = density, longitudinal velocity component and thickness, respectively, of the bottom layer;
n = Manning friction coefficient.

C. Mass Fluxes

The mass fluxes of salt and suspended sediment are 0 through the free surface and bottom, i.e.,:

$$(\varepsilon_z \frac{\partial s}{\partial z})_T = 0, \quad (\varepsilon_z \frac{\partial c}{\partial z})_T = 0 \qquad \text{for the top layer}$$

and

$$(\varepsilon_z \frac{\partial s}{\partial z})_b = 0, \quad (\varepsilon_z \frac{\partial c}{\partial z})_b = 0 \qquad \text{for the bottom layer.}$$

V. Finite Difference Formulation

With the grid system of *Figure 4,* the longitudinal advection term can be expressed in a form that allows for the conservation of energy [Leendertse et al., 1973]. The two independent variables x and t are set at equally spaced finite intervals of Δx and Δt, respectively. Using i and k to represent the number of intervals in the x and z directions, respectively, and using n to denote the number of time intervals that has elapsed, variables will be represented using i, k, n subscripts where $i, k,$ or $n = 0, 1, 2, 3, \ldots$. Exceptions are the estuary width B (a function of x and z only), the surface elevation η (a function of x and t only), and the layer thickness h (a function of t for the surface layer and a function of z only for the other layers).

The finite difference formulas are written using the operators of Shuman [1962]:

$$\overline{F}^x = \frac{1}{2}(F_{i,k,n} + F_{i+1,k,n}),$$

$$\delta_x F = \frac{1}{\Delta x}(F_{i+1,k,n} - F_{i,k,n}),$$

where F is a dependent variable. These operators are shown for x, with operators similarly defined for z and t. To denote a shifted time interval, the notation used is:

$$F_+ = F_{i,k,n+1} \text{ and } F_- = F_{i,k,n-1}$$

The finite difference approximations of equations 12, 13, 14, 15, and 16 are:

continuity equations—

$$\overline{\delta_t \eta}^t = \frac{1}{B_1}\left(w_1 \bar{B}_1^z - \delta_x(u\bar{B}^x\bar{h}^x)_1 + q_1 \cdot h_1\right) \tag{23}$$

$$h\delta_z(\bar{B}^z w) = -\delta_x(u\bar{B}^x\bar{h}^x) + q_k \cdot h_k \tag{24}$$

equation of motion—

$$\begin{aligned}\overline{\delta_t(u\bar{h}^x\bar{B}^x)}^t = &-\delta_x\,\overline{(\bar{B}^x\bar{h}^x u\,\bar{u}^x)}^x - \bar{h}^z\,\delta_z\,(\bar{u}^z\bar{w}^x\bar{B}^{xz}) \\ &- \frac{\bar{B}^x\bar{h}^x}{\bar{\rho}^x} \cdot \left(\frac{\partial P}{\partial x}\right)_k + \delta_x\overline{(\bar{B}^x\bar{h}^x e_x\,\delta_x u)}^x - \\ &+ \bar{h}^z\delta_z\,(\overline{e_z}^x\,\bar{B}^{xz}\delta_z u)_- + q\,u_t\,h\end{aligned} \tag{25}$$

mass-balance equation for salt—

$$\begin{aligned}\overline{\delta_t(sh\,B)}^t = &-\delta_x(\bar{B}^x\bar{h}^x\bar{s}^x u) - h\,\delta_z\,(w\,\bar{s}^z\bar{B}^z) \\ &+ \delta_x(E_x\bar{B}^x\bar{h}^x\delta\,s)_- + h\,\delta_z\,(E_z\bar{B}^z\delta_z s)_- \\ &+ q \cdot s_t h\end{aligned} \tag{26}$$

mass-balance equation for sediment—

$$\begin{aligned}\overline{\delta_t(ch\,B)}^t = &-\delta_x(\bar{B}^x\bar{h}^x c\,u) - h\,\delta_z\,((w-V)\bar{c}^z\bar{B}^z) \\ &+ \delta_x(E_x\bar{B}^x\bar{h}^x\delta_x c)_- + h\,\delta_z\,(E_z\bar{B}^z\delta_z c)_- \\ &+ q\,c_t h - Bd + B\,r\end{aligned} \tag{27}$$

These finite difference equations in the compact notation are used here for the purposes of derivation and presentation. The expanded forms—actually used for programming the model—are presented in the *Appendix,* p. 69.

VI. Mass and Momentum Exchange Coefficients

Bowden and Hamilton [1975] have reviewed the various formulations by which the vertical mass and momentum exchange coefficients may be related to the density stratification of water column. In general, they have the following forms:

$$\varepsilon_z = \nu_o (1 + \beta Ri)^p \tag{28}$$

$$e_z = \nu_o' \ (1 + mRi)^q \tag{29}$$

where ν_o and ν_o' are the values in homogeneous flow field; β, m, p, and q are constants to be determined empirically, and Ri is the Richardson number defined by:

$$Ri = - \frac{g}{\rho} \frac{\frac{\partial \rho}{\partial z}}{(\frac{\partial u}{\partial z})^2}$$

For the model used in this study, the empirical formula suggested by Pritchard [1960] is used. The formula was developed for mass exchange coefficient by fitting the observational results in the James River estuary. The effects of wind and stratification are included:

$$\varepsilon_z = (\nu_o + \nu_w) \ (1 + 0.276 \ Ri)^{-2} \tag{30}$$

In the equation, ν_o represents the mass exchange coefficient in a homogeneous flow field, given by:

$$\nu_o = \frac{8.59 \times 10^{-3} |u| \{z(h'-z)\}^2}{h'^3} \tag{31}$$

and ν_w' represents the exchange coefficient resulting from the mixing by wind-induced waves, given by:

$$\nu_w = 9.57 \times 10^{-3} \frac{z(h'-z)H}{h'T} \cdot \exp(- \frac{2\pi z}{L}) \tag{32}$$

where:

z = depth at which ϵ_z is being calculated;
h' = total depth of water;
H = wave height;
T = wave period;
L = wave length.

For the vertical momentum exchange coefficient, ν_o' and m are assumed to be of the same values as ν_o and β, respectively, while q is taken to be -½.

Compiling the published data, Dyer [1973] suggested that the horizontal exchange coefficients are of the order 10^5 of the vertical exchange coefficients. Festa and Hansen [1976] altered the momentum exchange coefficient e_x from $e_x = e_z$ to $e_x = 10^6 \cdot e_z$ with negligible effects on the results of their tidal average model. This indicates that the exact value of e_x is not critical. Festa and Hansen did find that varying the mass exchange coefficient ϵ_x from $\epsilon_x = \epsilon_z$ to $\epsilon_x = 10^7 \cdot \epsilon_z$ did produce significant changes in their results. Using Dyer's data as a basis, $e_x = 10^5 \cdot e_z$ and $\epsilon_x = 10^5 \cdot \epsilon_z$ are used for this model.

In the finite difference formulation, the grid points at which e_z and ϵ_z are determined are those points at which the vertical velocity w is calculated. This leads to the following formulas used in calculating $(e_z)_{i,k,n}$ and $(\epsilon_z)_{i,k,n}$:

$$Ri = - \frac{g \, \delta_z \, \rho_-}{\bar{\rho}_-^z (\delta_z u_-)^2} \qquad (32)$$

$$\nu_o = \frac{8.59 \times 10^{-3} \{ (\sum_{j=1}^{k} h_j + \eta_{i,n-1}) (\sum_{j=k+1}^{k_i} h_j) \}^2}{(\sum_{j=1}^{k_i} h_j + \eta_{i,n-1})^3} \qquad (33)$$

$$\nu_w = \frac{9.57 \times 10^{-3} \left(\sum_{j=1}^{k} h_j + \eta_{i,n-1} \right) \left(\sum_{j=k+1}^{k_i} h_j \right) H}{\left(\sum_{j=1}^{k_i} h_j + \eta_{i,n-1} \right) T} \cdot \exp\left\{ - \frac{2\pi \left(\sum_{j=1}^{k} h_j + \eta_{i,n-1} \right)}{L} \right\} \tag{34}$$

where k_i is the total number of layers at the ith transect. The values of variables η, u, and ρ at the previous time step are used since otherwise the numerical computation might become unstable [Leendertse et al., 1973].

The grid points at which e_x and ϵ_x are determined are those at which the horizontal velocity u is calculated. This gives the following formulas:

$$e_x = 10^5 \cdot \overline{\overline{e_z^x}}^z \tag{35}$$

$$\epsilon_x = 10^5 \cdot \overline{\overline{\epsilon_z^x}}^z \tag{36}$$

VII. Sediment Deposition and Resuspension Rates

As previously noted for equation 16, the variables d and r are non-0 only for the bottom layer of a transect. The resuspension term r acts as a source when the velocity shear at the bottom (i.e., the bed shear) becomes great enough to cause bed erosion. The deposition term d acts as a sink when the bed shear is low enough to allow sediment deposition.

The resuspension rate from surface erosion is given by Parthenaides [1962] as:

$$\begin{aligned} d &= M\left(\frac{\tau}{\tau_e} - 1\right) && \text{if } \tau > \tau_e \\ \text{or} \quad d &= 0 && \text{if } \tau \leq \tau_e \end{aligned} \Bigg\} \tag{36}$$

where:

τ = bed shear stress;
τ_e = critical shear stress which must be exceeded before erosion can occur;
M = a constant, equal to the rate of erosion at $\tau = 2\tau_e$.

Flume tests of Thames estuary mud [Hydraulic Research Station, 1970] containing a fair proportion of silt particles, showed that τ_e ranged from 2 to 5 dyne/cm^2. The study by Parthenaides [1965] indicated that M ranged from 2.75 x 10^{-7} to 3.5 x 10^{-7} gm/cm^2/sec. τ_e and M are read in as input parameters for this model, using the above numerical values as initial guidelines.

Extensive studies have been conducted by Krone [1962] and Parthenaides [1962] on the deposition of cohesive sediments. Krone postulated that the probability P of a particle sticking to the bed increases linearly from 0 to unit as the bed shear falls below the critical value τ_d, i.e.:

$$P = 1 - \frac{\tau}{\tau_d} \qquad \text{if } \tau < \tau_d \quad \} \tag{37}$$

or $P = 0 \qquad \text{if } \tau \geq \tau_d$

Therefore, the deposition rate may be written as:

$$d = Vc \left(1 - \frac{\tau}{\tau_d}\right) \tag{38}$$

where:

c = sediment concentration at the bottom layer;
V = falling velocity.

Flume tests of Thames mud by the Hydraulic Research Station [1970] showed that the value of τ_d is about 0.6 dyne/cm^2. This value is used as the initial guideline for the parameter in this model.

VIII. Settling Velocity

Samples of suspended sediment from the turbidity maximum zone in the Rappahannock Estuary have measured Stokes' diameters of <60 microns. Stokes' Law may be considered valid for spheres of diameters ≤62.5 microns in quiescent waters [Sverdrup et al., 1942]. As pointed out by Sverdrup, turbulent diffusion in the water column can cause an increase or a decrease in the downward transport due to settling. Since Stokes' Law was derived without consideration for turbulence, V should be altered to reflect estuarine turbulent conditions. Unfortunately, experiments involving sized particles (<1 mm) have not been conducted to discover those relationships between turbulence and settling velocities

predicted by Stokes' Law. Thus, the only theoretical basis on which settling velocities for spheres of diameters $\leqslant 62.5$ microns can be calculated is Stokes' Law:

$$V = \frac{1}{18\nu} \cdot \frac{\rho_s - \rho}{\rho} g D^2 \tag{39}$$

where:

ρ_s = density of sediment particle;
ρ = density of water;
ν = kinematic viscosity of water;
D = Stokes' diameters of particles.

Stokes' Law shows that the settling velocity of a sediment particle is not constant. Assuming ρ_s is constant for particles of all sizes and neglecting the density variation of estuarine water, the settling velocity may be considered to be proportional to the square of particle diameter, i.e.:

$$V(D) = KD^2 \tag{40}$$

where:

$$K = \frac{1}{18\nu} \cdot \frac{\rho_s - \rho}{\rho} g$$

To evaluate the vertical sediment fluxes—terms containing Vc in equations 27 and 38—the size-dependence of settling velocity has to be taken into account. Let $c(D)$ be the concentration of the sediment particles with a Stokes' diameter in the range D and $D + dD$, then:

$$\begin{aligned} V \cdot c &= \int_0^\infty V(D) \cdot c(D)\, dD \\ &= K \int_0^\infty D^2 \cdot c(D)\, dD \end{aligned} \tag{41}$$

Statistics give the variance of diameters of sediment particles as:

$$\theta^2 = \frac{\int_0^\infty (D - D_m)^2 \cdot c(D)\, dD}{c} \tag{42}$$

where the total concentration:

$$c = \int_0^\infty c(D)\, dD,$$

and the mean diameter:

$$D_m = \frac{1}{c} \int_o^\infty D \cdot c(D)\, dD$$

Equation 42 gives:

$$\int_o^\infty D^2 \cdot c(D)\, dD = c(\theta^2 + D_m^2) \tag{43}$$

and, thus:

$$V \cdot c = K(D_m^2 + \theta^2) \cdot c \tag{44}$$

which is used in the mass-balance equation for suspended sediment. The variation of K with time is small, and therefore, K is assumed to be constant over a tidal cycle. The same assumption is made for θ^2 and D_m^2. Sampling along the extent of the turbidity maximum in the Rappahannock Estuary, December 15, 1975, resulted in an average diameter of 6.53 microns and a mean variance of 59.6 *(Figures 5* and *6).*

IX. Numerical Treatment of Boundary Conditions

A. Landward Boundary

The landward boundary of the model is chosen at the fall line or landward limit of tidal influence. It is assumed that the fresh water and sediment discharge are known at this landward boundary. Therefore, the velocity and sediment concentration are specified at the most landward transect, i.e.:

$$U_{2,k} = Q(t)/A$$

$$C_{2,k} = M(t)/Q(t) \qquad \text{for all } k.$$

where:

subscript

2 = transect number two (the most landward transect);

$Q(t)$, $M(t)$ = fresh water and sediment discharge, respectively;

A = cross-sectional area.

Since the salt intrusion is usually limited to the seaward half of the tidal

portion of the Rappahannock Estuary, the salinity at the landward boundary is specified to be 0, i.e.:

$$S_{2,k} = 0 \qquad \text{for all time.}$$

B. Seaward Boundary

The seaward boundary is located at the mouth of estuary. The surface elevation at the seaward-most transect is specified with a harmonic function:

$$\eta_j\ (t) = \eta_o \sin\ (2\pi \frac{t}{T}) \tag{45}$$

where:

T = tidal period;

η_o = tidal amplitude found from tide tables;

subscript

j = transect number j, the most downstream transect.

Two methods are investigated for calculating velocities near the open boundary. The first assumes that the dominant momentum balance takes place between the effects of surface slope, density gradient, internal and bottom friction. The horizontal diffusion and advection of momentum are neglected at the mouth. Alternatively, the horizontal velocities are linearly extrapolated to a fictitious transect out of the mouth, and the advective and diffusive terms are included as interior transects. The difference between the results of the two methods is negligible. The latter method is adopted for the model.

An "oceanic" or "bay" salinity is assumed to exist off of the mouth of the estuary. At flood tide, it is assumed that the bay water is advected into the estuary, and the salinity at the seaward boundary becomes equal to the bay salinity. To account for the incomplete mixing in the bay, Thatcher and Harleman [1972] suggested that some period of adjustment should be allowed after the flow started to flood and before the salinity at the mouth reached the bay value. In this model, an input parameter is assigned for the specification of this adjustment period, and the salinity is assumed to increase linearly with time during this period.

At ebb tide, the horizontal salinity profile is assumed to have advected out of the mouth as a "frozen" pattern, i.e., neglecting the diffusion.

Numerically, the salinity at the seaward transect was calculated as:

$$s_{j,k}(t + \Delta t) = s_{j,k}(t) - \frac{s_{j,k}(t) - s_{j-1,k}(t)}{\Delta x} \cdot u_{j,k}(t) \cdot \Delta t \qquad (46)$$

The seaward boundary condition for the suspended sediment is treated the same way as that of the salinity.

X. Procedures for Numerical Calculation

Starting with all the variables assigned at their initial values, the explicit scheme is used to solve the finite difference equations 23, 24, 25, 26, and 27. At the nth time step, the continuity equation for the top layer (equation 23) is used to calculate $\eta_{i,n+1}$. With $\eta_{i,n+1}$ known, $u_{i,k,n+1}$, $s_{i,k,n+1}$, and $c_{i,k,n+1}$ can be calculated for all i's and k's using equations 25, 26, and 27. Knowing all the u's for the $(n + 1)^{st}$ time step allows all the w's for the $(n + 1)^{st}$ time step to be calculated using equation 24.

Next, the density, pressure gradients, and the eddy viscosity and turbulent diffusion coefficient are calculated for the $(n + 1)^{st}$ time step. At this point, the entire sequence above is repeated to calculate the values of the variables at the $(n + 2)^{nd}$ time step. A brief flow chart summarizing the sequence of numerical calculations is shown in *Figure 7.*

XI. Computational Tests

Several computational tests were conducted to assure that the proper governing equations had been formulated correctly in the numerical program. The physical problem for the tests is the reflection of a tidal wave propagating into a closed-end channel of uniform rectangular cross-section. The following parameters are used in the model:

length of channel = 97.5 km;
depth of channel = 10 m;
amplitude of incoming tidal wave = 10 cm;
period of tidal wave = 12 hours;
wave length = 427.7 km;
Δx = 5 km;
Δz = 2 m;
Δt = 240 seconds.

All computations are started with initial conditions of velocity = 0 and tidal height = 0 throughout the channel. The ocean salinity is set to 0 at all depths so that salinity effects are not included in the tidal dynamics. The computation proceeds with the water surface elevation at the channel entrance varying in simple harmonic motion while the velocity at the closed end of the channel is kept constantly at 0.

The model is run first with a Manning friction coefficient of 0.015. Several values of time step Δt were tried, and it was found that a time step greater than six minutes will cause the numerical computation to become unstable. A time step of four minutes was found to be optimal for the test run and it was used for all the computational tests. The model was run for a time equivalent of 12 tidal cycles to assure the establishment of the tidal regime. The resulting time-varying tidal height and surface current are shown in *Figures 8, 9* and *10* for locations at the channel entrance, at the mid-point of the channel, and near the closed end. These *Figures* show that all of the initial transients have been damped out by the eighth tidal cycle. *Figures 11* and *12* show the longitudinal variation of tidal amplitude and vertically-averaged tidal current. Theoretical curves based on the linear frictionless model [Ippen, 1966] are presented in the *Figures.*

The model also was run with a Manning friction coefficient 0.010, and the results of tidal amplitude and current are shown in *Figures 11* and *12.* The model agrees with the theory: the predicted tidal amplitude and tidal current are smaller than the frictionless theory, and the model results approach the theoretical results when the friction coefficient is decreased. Since no analytical solution exists for the non-linear friction model, the numerical results cannot be tested quantitatively.

XII. Numerical Simulation

The model simulates only the tidal portion of the river, considering the fluvial input as the headwaters or principal freshwater and sediment sources. The U.S. Corps of Engineers measured cross-sectional profiles of some 100 transects along the tidal portion of the river. These profiles were used to schematize the river with Δx = 5 km, Δz = 2 m. *Figure 13* shows the longitudinal segmentation of the river; *Figure 14* is a schematized vertical profile. A time step increment of 240 seconds is used for all the model runs.

The free surface height at the ocean boundary is a pure sine wave with an amplitude equal to half mean range at Stingray Point (18.3 cm) and a period of 12 hours. Two simulations were tested; one corresponds to high freshwater inflow and the other corresponds to low inflow condition. The boundary conditions are obtained or estimated from the available field data:

Upstream Boundary Conditions	Low Flow (23 m^3/sec)	High Flow (122 m^3/sec)
Velocity	10 cm/sec	53 cm/sec
Salinity	0 ppt	0 ppt
Sediment Concentration	40 mg/l	132 mg/l
Downstream Boundary Conditions		
Salinity	16 ppt (uniform)	surface 14 ppt bottom 16 ppt
Sediment Concentration	0	0

The initial condition on the salinity field is a linear distribution from mouth to the mid-point of the tidal river, and the initial condition on the velocity field is the river discharge divided by the cross-sectional area of the grid point. The free surface height is initially a level surface. The initial sediment concentration field is a linear distribution from the upstream boundary to the mouth. The simulation is carried out for 10 tidal cycles and the results of the last tidal cycle are presented.

XIII. Tidal Characteristics

Figures 15 and *16* show the computed tidal range and the predicted mean range tabulated from the tide tables [National Ocean Survey, 1977]. Both the model and tide data show that the tidal range increases upstream from the river mouth, reaching a local maximum at Bowlers Rock (55 km from mouth). At this point, the model over-estimates the range by six percent. Maximum tide range occurs at Fredericksburg, the head of the tidal estuary, whereas a minimum occurs near Leedstown (about 100 km from mouth). This is a characteristic standing wave which results from superposition of two progressive waves traveling in opposite directions. The outgoing reflected wave is out of phase with respect to the incoming wave at a distance of quarter wave length from the head of tide. It results in a nodal point of minimum tidal range at Leedstown. The model reproduces this characteristic quite well.

When the tide range at different river inflows is compared *(Figures 15* and *16),* it is seen that high river discharge affects tidal range only near the extreme head of tide. High river inflow retards the tidal wave propagation and reduces the tidal range, landward of 140 km.

The phase lags along the river are demonstrated in *Figures 17* and *18* for the cases of low and high river flows, respectively. The model predicts a larger difference in phase speeds at high and low tides.

Figures 19 and *20* compare the tidal stage and surface current at various stations along the river. The tide changes its characteristics as it propogates upstream. At the estuary mouth (station 36), the tidal wave is a progressive wave in the sense that the tidal stage is nearly in phase with tidal current. The tidal current leads more and more with respect to the tidal height as the wave propagates upstream. Near the head of tide (station 2), the phase relationship is marked by the existence of net downstream velocity due to river discharge.

XIV. Estuarine Circulation

The most important aspect of the estuarine circulation which must be modeled is the gravitational circulation [Hansen and Rattray, 1965]. The tidal average circulation in a coastal plain estuary is dominated by the upstream movement of heavier saline water in the lower layer and the downstream movement of fresher water in the upper layer. This circulation pattern is driven by the longitudinal gradient of salinity distribution.

Figures 21 and *22* show the tidally-averaged salinity and longitudinal velocity distribution (averaged over one tidal cycle) for high and low river inflow, respectively. For the case of high river discharge, the null point— the point where the line of no-net-motion meets the estuary bottom— is located at the head of salt intrusion, i.e., 1 ppt isohaline, as an indicator. Above the line of no-net-motion, the downstream net velocity increases seaward despite the enlargement of river cross-section in that direction. This augmentation of net flow rate is derived from the landward intrusion of Chesapeake Bay water through the mouth which often enhances the flushing capability of an estuary by an order of magnitude.

Figure 22 shows that saline water intrudes farther upstream when the river discharge is low. The null point also moves upstream, but fails to

reach the salt intrusion head. This is contrary to the general observation that the null point is located at the head of salt intrusion. It is suspected that the upstream net movement of water is retarded by a rise in the estuary bed. When a hypothetical situation of constant river depth is tested, the null point moves up and down the estuary with the head of salt intrusion in response to the river discharge.

XV. Turbidity Maximum

The tidally-averaged sediment concentration distributions, averaged over one tidal cycle, are shown in *Figure 23;* a local maximum concentration exists around the null point. This agrees qualitatively with field observations [Nichols, 1973], but the strength of maximum is much weaker than that observed. The results presented here are equilibrium conditions under constant river discharges, while the field observations are the sediment distributions that evolve after transient flow conditions. The stronger turbidity maximum may be due, at least partially, to the reduction of sediment source after the river flow subsides.

During the process of numerical simulation, it was noted that the suspended sediment distribution is quite sensitive to the vertical diffusion coefficient, settling velocity, critical shear stress of sediment deposition and resuspension, and the resuspension constant. The results presented here are taken from the test runs, with the following parameter values:

settling velocity, V = 2/3 of that calculated with Stokes' Law;
critical shear stress of deposition, τ_d = 0.3 dyne/cm^2;
critical shear stress of resuspension, τ_e = 0.5 dyne/cm^2;
resuspension constant, M = 0.3 μg/cm^2/sec.

Without independent determination of these parameters, the model can be used only for the qualitative interpretation of the sediment transport process. Determining the values of these parameters is an important research priority if the sediment transport process and generation of the turbidity maximum in estuaries are to be understood fully. The most interesting condition for developing the turbidity maximum is the transient high river inflow which introduces a pulse load of suspended sediment into the estuary. It would be most desirable to simulate this transient condition and to study the evolution of the turbidity maximum as the freshet comes and goes.

REFERENCES

Ariathurai, C. R., 1974. *A Finite Element Model for Sediment Transport in Estuaries.* Ph.D. dissertation. University of California, Davis.

Bowden, K. F. and Hamilton, P., 1975. "Some Experiments With a Numerical Model of Circulation and Mixing in a Tidal Estuary." *Estuarine and Coastal Marine Science* 3:281-301.

Byrne, R. and Anderson, G., 1977. *Shore Erosion in Tidewater Virginia.* Virginia Institute of Marine Science. SRAMSOE 111.

Caponi, E. A., 1974. *A Three-Dimensional Model for the Numerical Simulation of Estuaries.* University of Maryland, Institute of Fluid Dynamics and Applied Mechanics. Technical Note BN-800.

———, 1976. "A Three-Dimensional Model for the Numerical Simulation of Estuaries." *Advances in Geophysics* 19:189-310.

Christodoulou, G. C., Leimkuhler, W. F., and Ippen, A. T., 1974. *A Mathematical Model for the Dispersion of Suspended Sediments in Coastal Waters.* Report No. 179. Ralph M. Parsons Laboratory, Cambridge, Massachusetts.

Connor, D. O., 1977. Personal communication.

Dyer, K., 1973. *Estuaries: A Physical Introduction.* John Wiley, New York.

Eckart, C., 1958. "The Equations of State of Water and Sea Water at Low Temperatures and Pressures." *American Journal of Science* 256: 225-40.

Festa, J. F. and Hansen, D. V., 1976. "A Two-Dimensional Numerical Model of Estuarine Circulation: The Effects of Alternating Depth and River Discharge." *Estuarine and Coastal Marine Science* 4:309-23.

Festa, J. F., 1976. Personal communication.

Fischer, H. B., 1967. "The Mechanics of Dispersion in Natural Stream." *Proceedings, American Society of Civil Engineers* 93(HY6):187-216.

Hansen, D. V. and Rattray, M., Jr., 1965. "Gravitational Circulation in Straits." *Journal of Marine Research* 23: 104-22.

Harrison, A. J. M. and Owen, M. W., 1971. "Siltation of Fine Sediments in Estuaries." *Proceedings, Association of Hydraulic Research* 4:D1-1–D1-8.

Hunter, J. R., 1975. *A Three-Dimensional Kinematic Model of Suspended Sediment Transport in the Upper Chesapeake Bay.* Special Report 46. Chesapeake Bay Institute of Johns Hopkins University.

Hydraulics Research Station, 1970. *Thames Estuary Flood Prevention Investigation. Mathematical Silt Model Studies: The Effect of a Half Tide Barrier at Either Woolwich or Blackwall on Siltation in the Estuary.* Report No. EX 479. Wallingford, England.

Ippen, A., 1966. *Estuary and Coastline Hydrodynamics.* McGraw-Hill Book Company, Inc., New York.

Krone, R. B., 1962. *Flume Studies of the Transport of Sediment in Estuarial Shoaling Processes.* Final Report. Hydraulic Engineering Laboratory, University of California, Berkeley.

———, 1963. *A Study of Rheologic Properties of Estuarial Sediments.* Technical Bulletin No. 7. Final contract report to U.S. Army Corps of Engineers, Committee on Tidal Hydraulics.

Leendertse, J. J., Alexander, R. C., and Liu, Shiao-kung, 1973. *A Three-Dimensional Model for Estuaries and Coastal Seas. Volume 1: Principles of Computation.* Rand Contract Report R-1417-OWRR.

Meade, R. H. and Trimble, S. W., 1974. "Changes in Sediment Loads in Rivers of the Atlantic Drainage of the United States Since 1900." *Proceedings, International Association of Hydraulic Research* 113:99-104.

National Ocean Survey, 1977. *Tide Tables 1977.* National Oceanic and Atmospheric Administration, U.S. Department of Commerce.

Nichols, M. and Thompson, G., 1973. *Development of the Turbidity Maximum in a Coastal Plain Estuary.* Virginia Institute of Marine Science Special Scientific Report 75.

Odd, N. V. M. and Owen, M. W., 1972. "A Two-Layer Model of Mud Transport in the Thames Estuary." *Proceedings, Institution of Civil Engineers, London.* Paper 75175: 175-205.

Parthenaides, E., 1962. *A Study of Erosion and Deposition of Cohesive Soils in Salt Water.* Ph.D. dissertation. University of California, Berkeley.

———, 1965. "Erosion and Deposition of Cohesive Soils." *Journal of the Hydraulics Division, Proceedings, American Society of Civil Engineers.* Vol. 91, No. HY1, Paper 4204.

Postma, H., 1969. "Marine Pollution and Sedimentology." *Pollution Symposium.* pp. 225-34. Texas A & M University.

Pritchard, D. W., 1960. "The Movement and Mixing of Contaminants in Tidal Estuaries." *Waste Disposal in the Marine Environment.* pp. 512-25. Pergamon Press, New York.

Schubel, J. and Carter, H.H., 1977. "Suspended Sediment Budget for Chesapeake Bay." *Third Estuarine Research Federation Conference.* Galveston, Texas.

Shuman, F. G., 1962. "Numerical Experiments With the Primitive Equations." *Proceedings, International Symposium on Numerical Weather Prediction.* pp. 85-107. Tokyo, Meteorological Society of Japan.

Sverdrup, H. V., Johnson, M. W., and Fleming, R. H., 1942. *The Oceans.* Prentice-Hall, New York.

Thatcher, M. L. and Harleman, D. R. F., 1972. *A Mathematical Model for the Prediction of Unsteady Salinity Intrusion in Estuaries.* Massachusetts Institute of Technology Report No. 72-7.

FIGURES

FIGURE 1

Variations of Suspended Sediment Concentration and Current Speed over Two Tidal Cycles, April 5-6, 1970; Station 22 in the Turbidity Maximum—Rappahannock Estuary

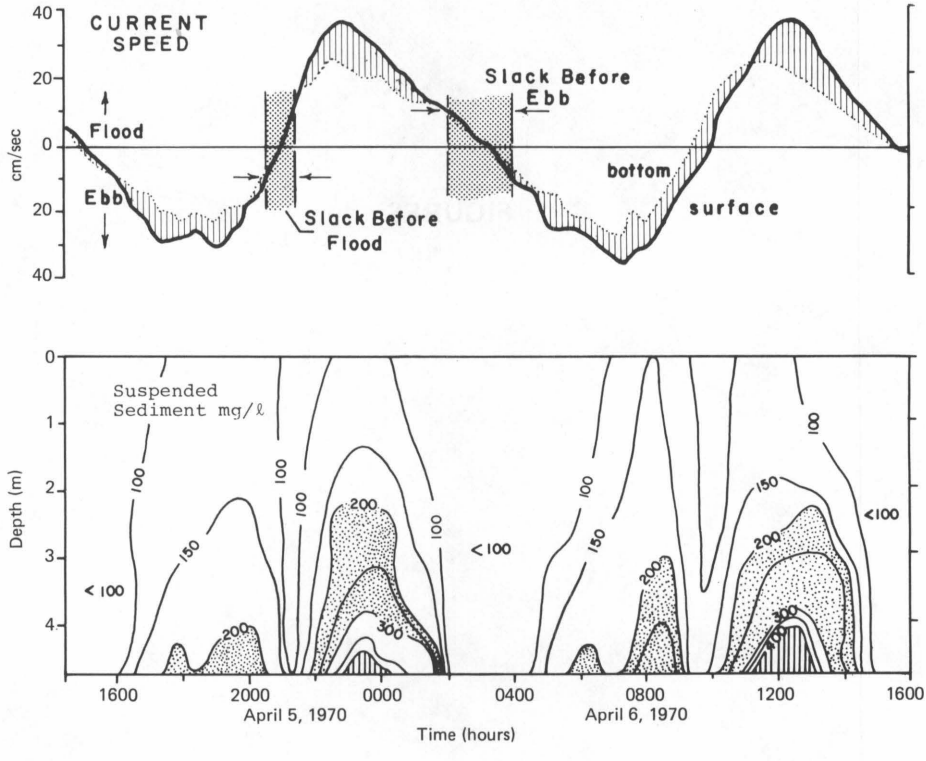

FIGURE 2

Longitudinal Distribution of Net Velocity
Near the Bottom through the Middle Rappahannock Estuary,
Showing Null Zone Where Velocities Approach Zero
(From Observations of April 1-15, 1970)

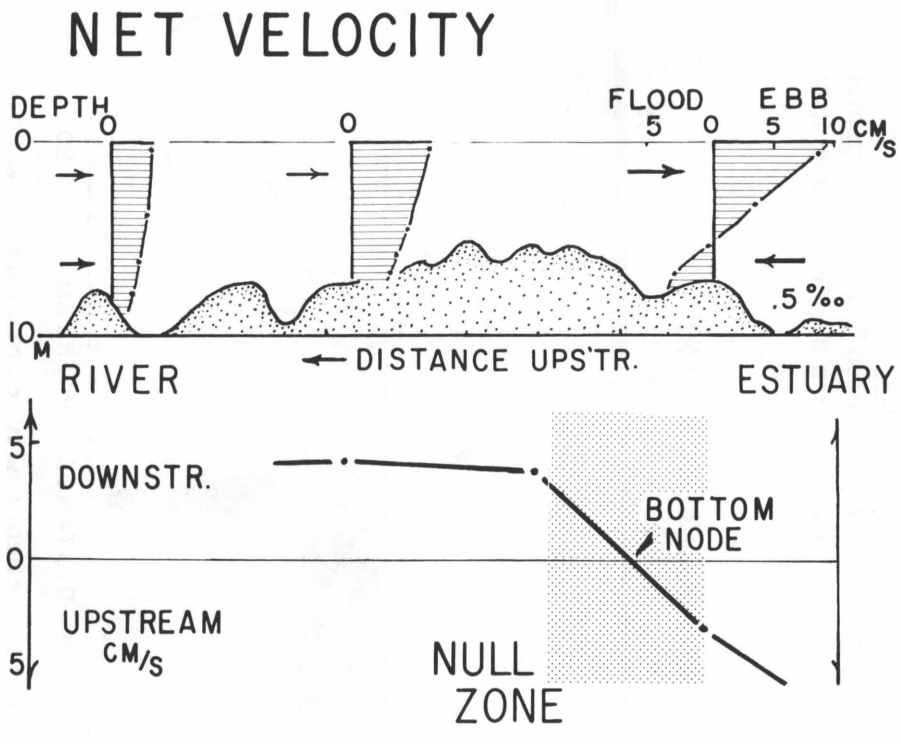

FIGURE 3

Longitudinal Distribution of Suspended Sediment Concentration Which Forms a Turbidity Maximum in the Middle James Estuary

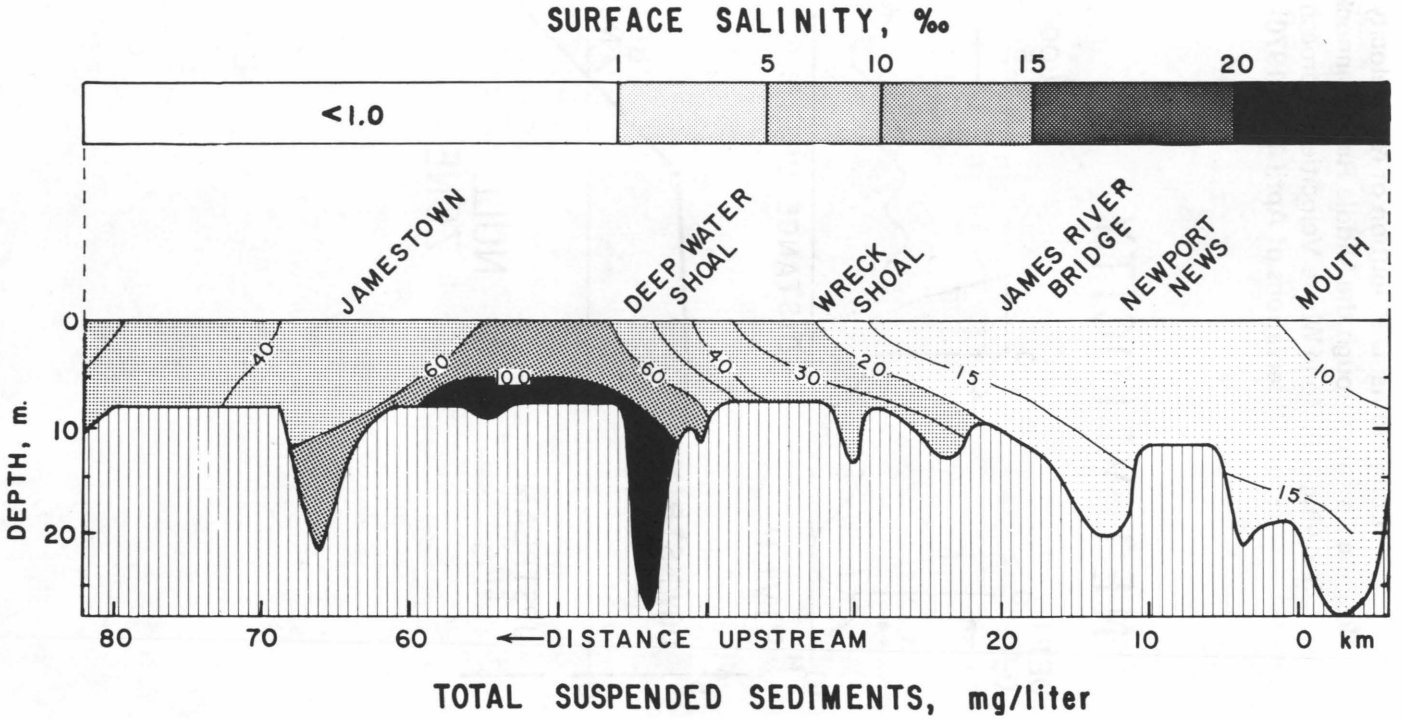

FIGURE 4
Grid Pattern, Location and Indexing of Variables

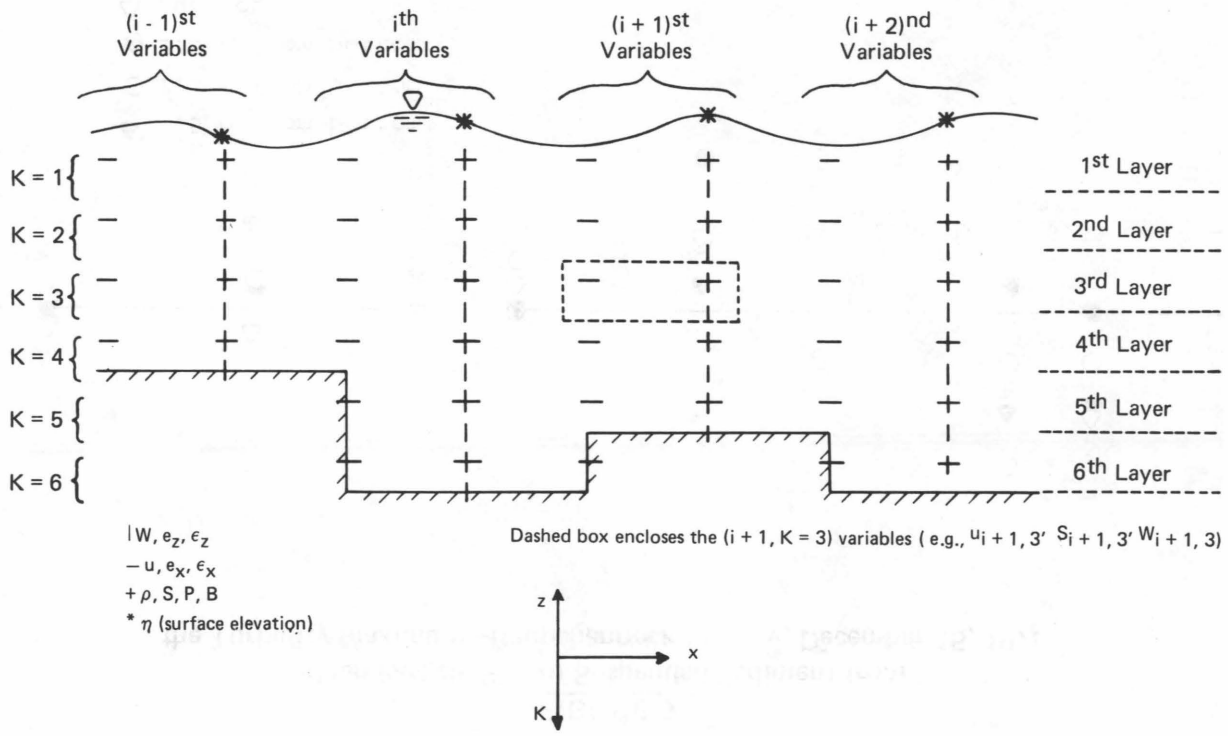

FIGURE 5

Mean Particle Size of Suspended Sediment from the Turbidity Maximum—Rappahannock Estuary, December 15, 1975

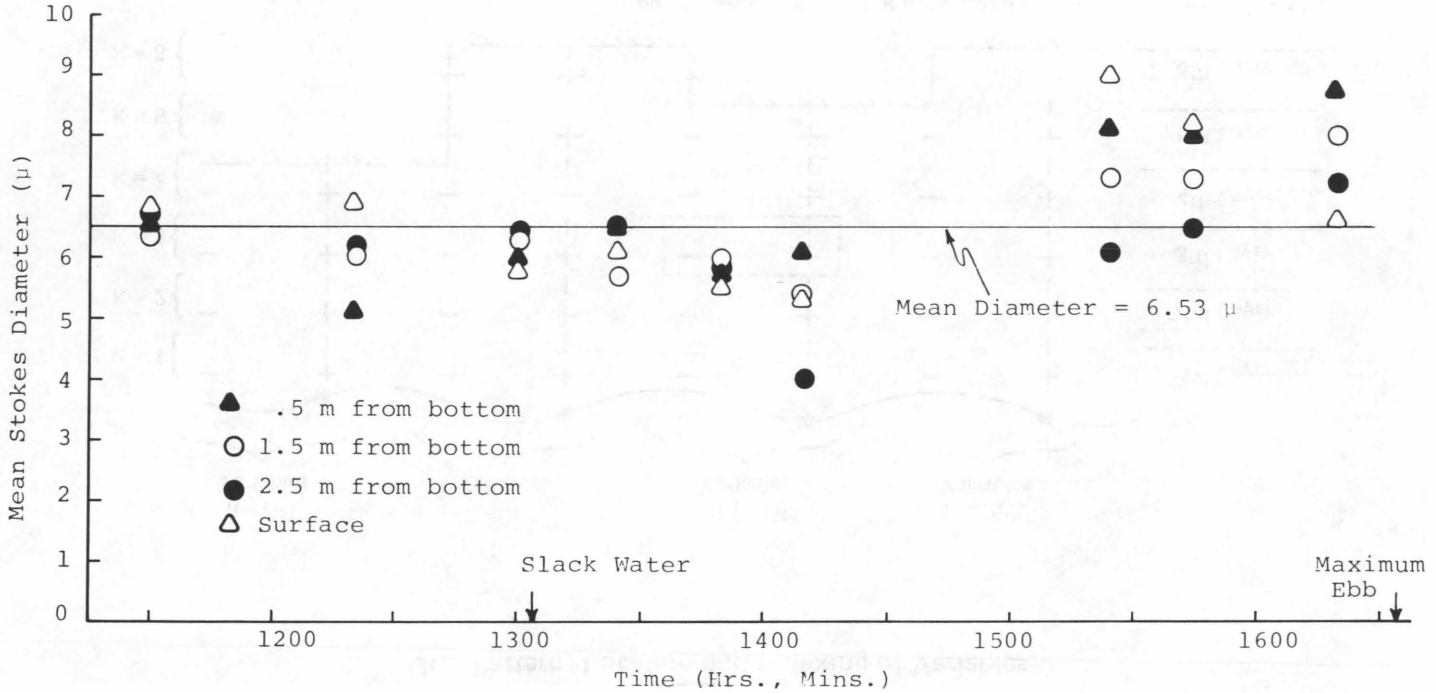

FIGURE 6

Variance of Particle Size of Suspended Sediment from the Turbidity Maximum—Rappahannock Estuary, December 15, 1975

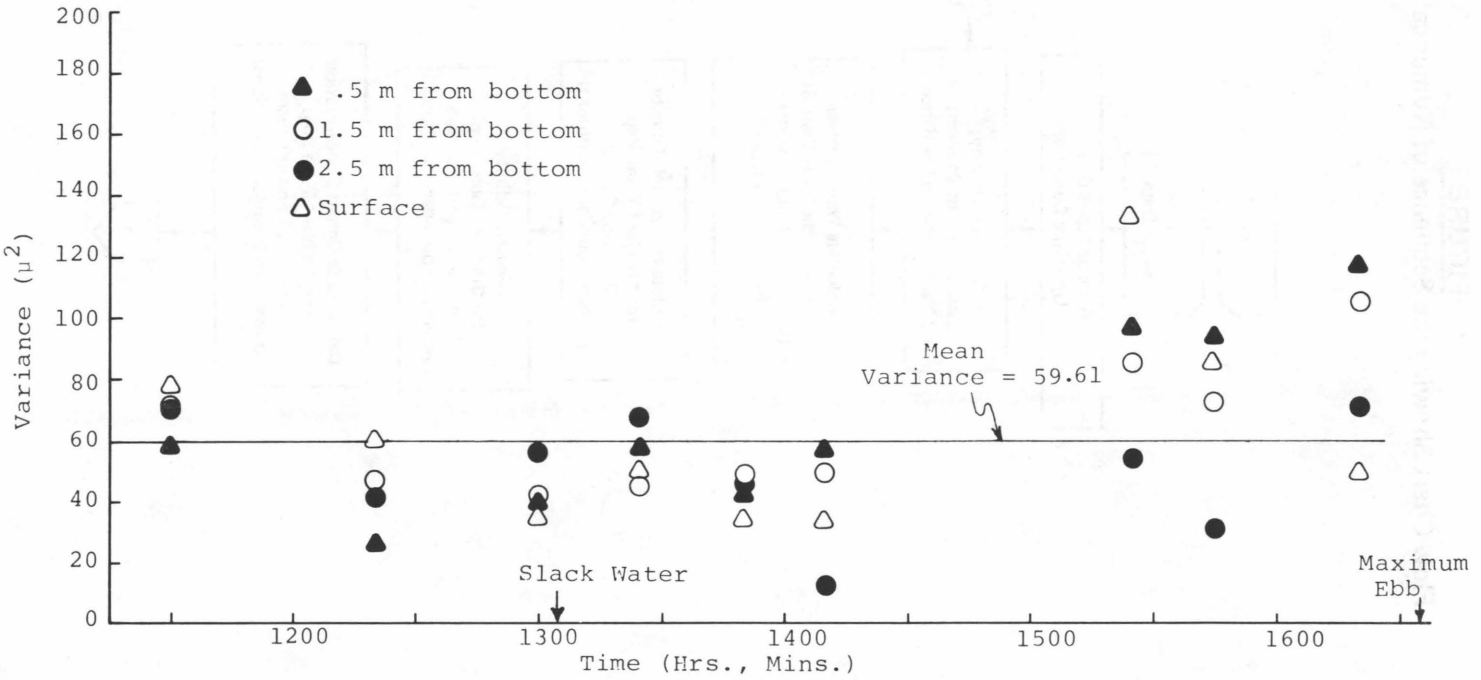

FIGURE 7

Flow Chart Showing the Sequence of Numerical Calculation

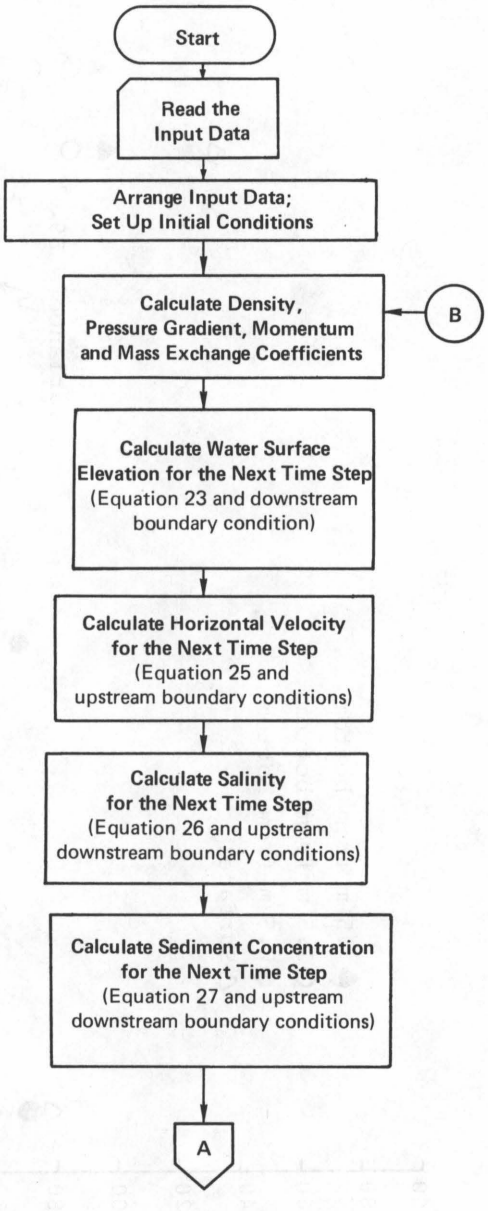

FIGURE 7 (continued)

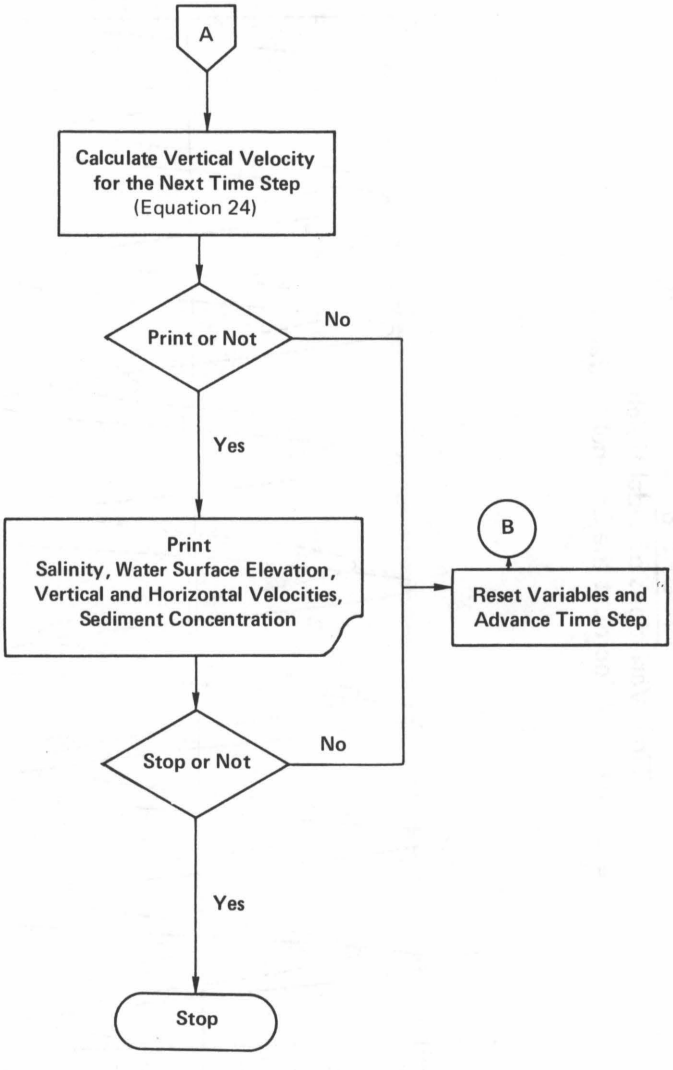

FIGURE 8
Time Variations of Tidal Height and Surface Velocity at the Channel Entrance

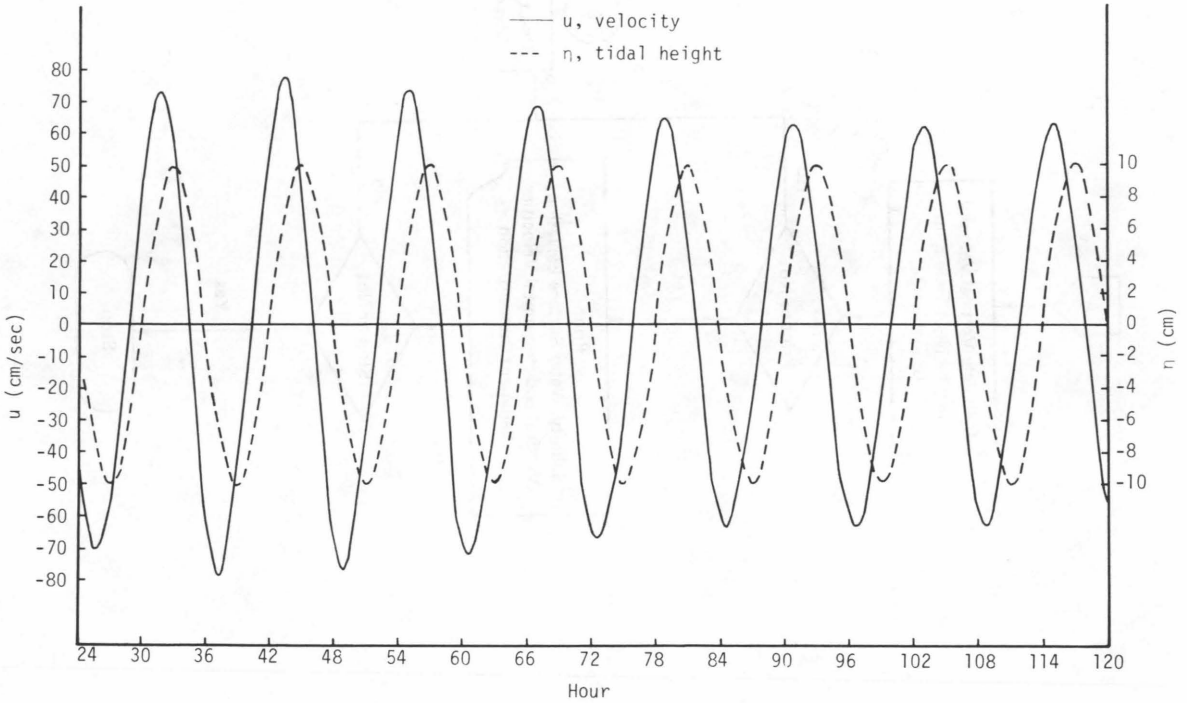

*η = 0.015; transect 21.

FIGURE 9

Time Variations of Tidal Height and Surface Velocity at the Mid-Point of the Channel

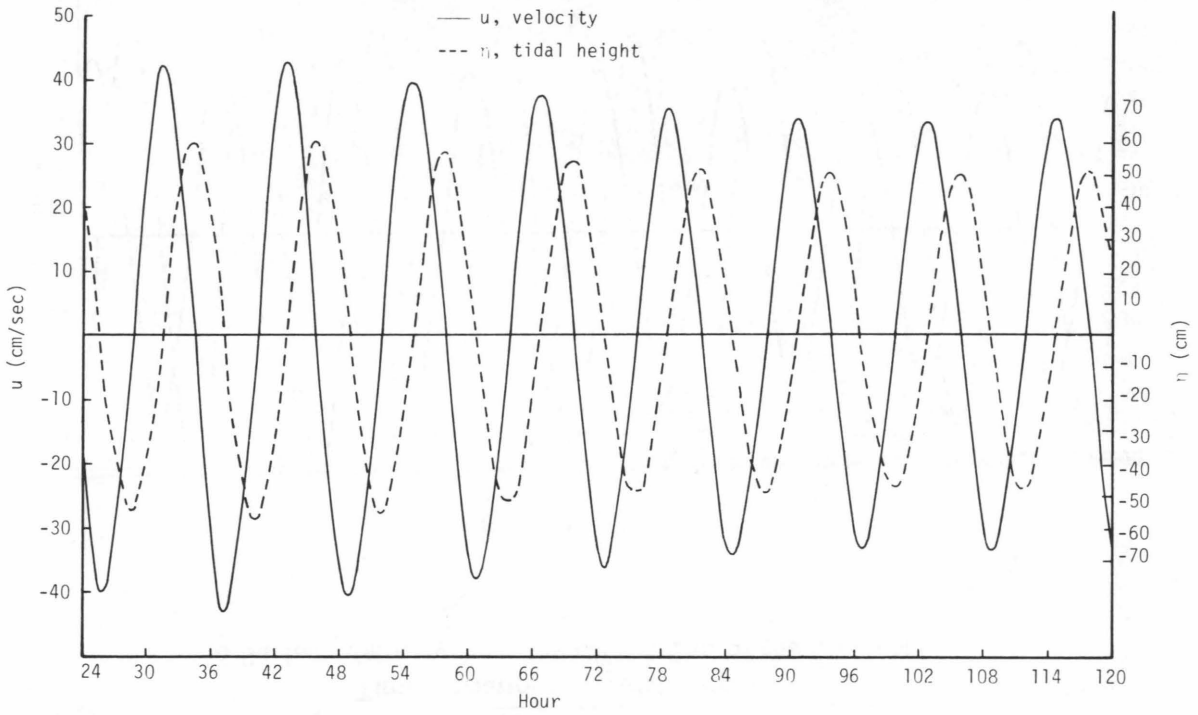

*η = 0.015; transect 10.

FIGURE 10
Time Variations of Tidal Height and Surface Velocity Near the Closed End of the Channel

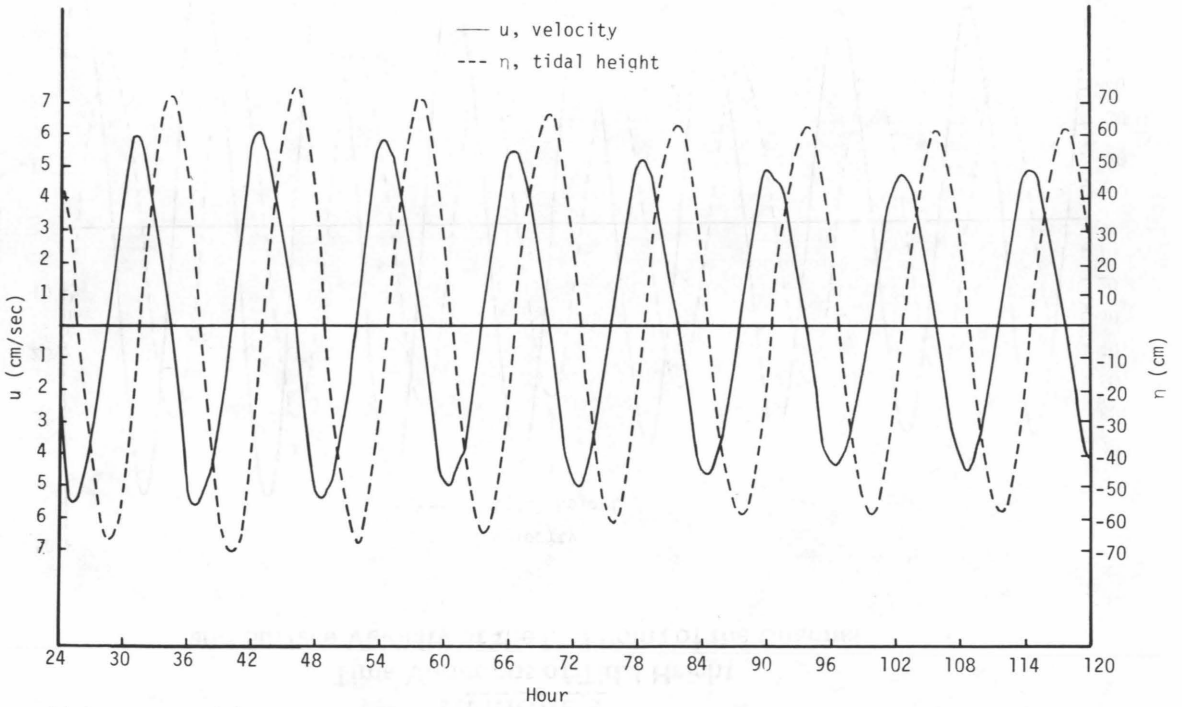

*η = 0.015; transect 2(η); transect 3(η).

FIGURE 11
Longitudinal Distribution of Tidal Amplitude Along a Closed-End Channel

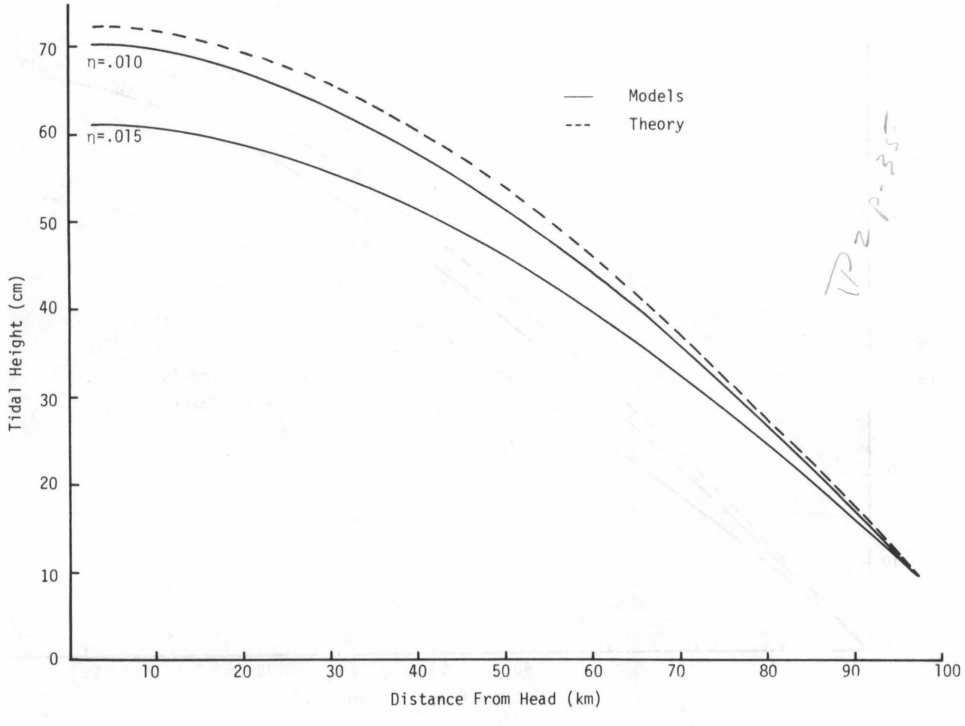

FIGURE 12

Longitudinal Distribution of the Amplitude of Tidal Current Along a Closed-End Channel

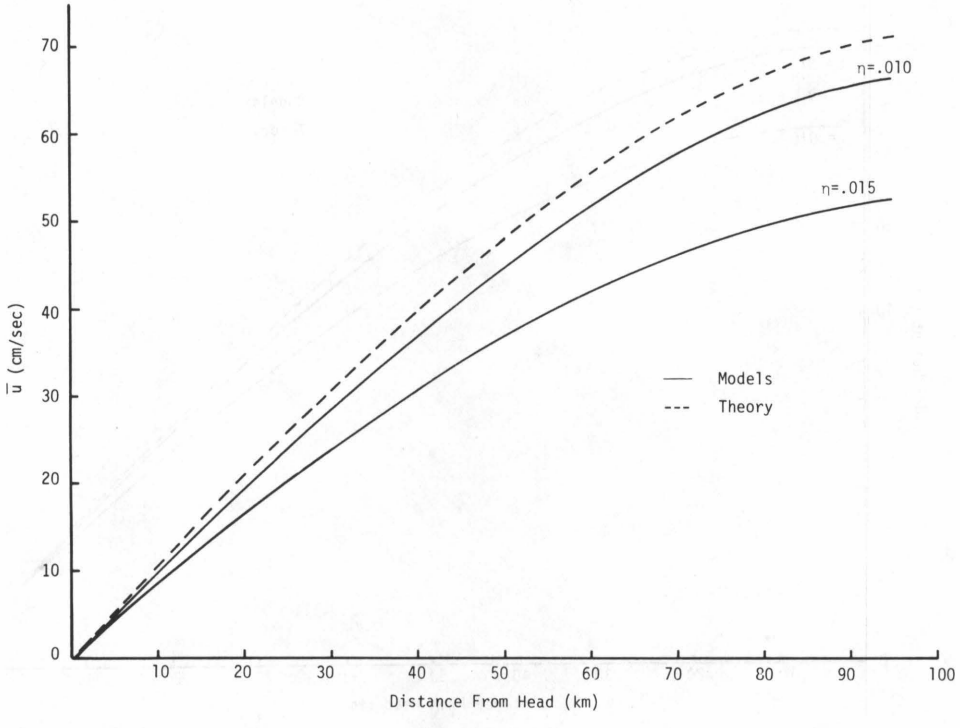

FIGURE 13

Location of the Rappahannock River–
Lower Inset and Longitudinal Segmentation Scheme

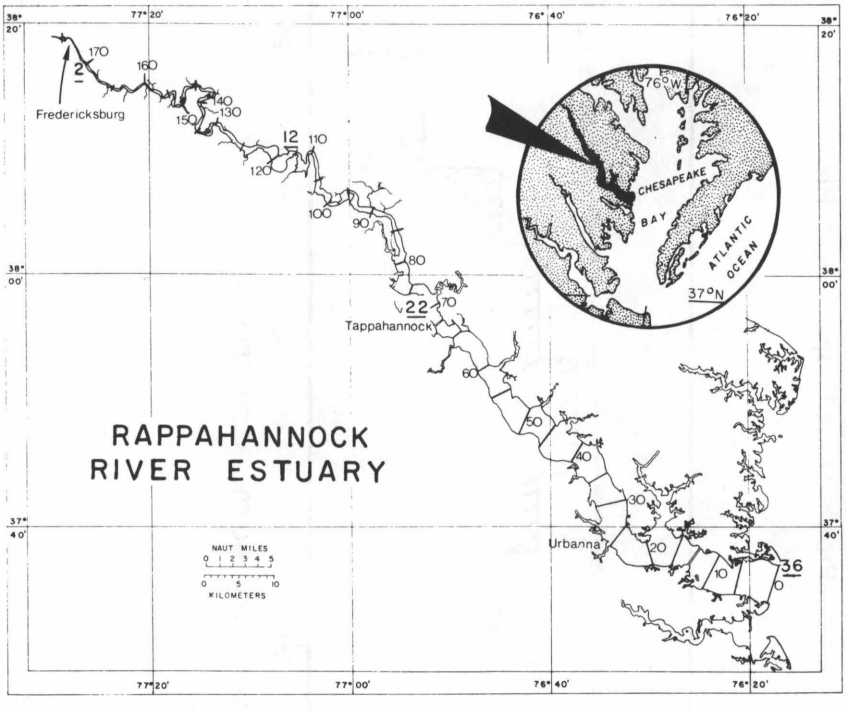

*Numbers are kilometers upstream from the mouth, and station locations, underlined.

FIGURE 14
Schematized Bottom Profile of the Rappahannock River

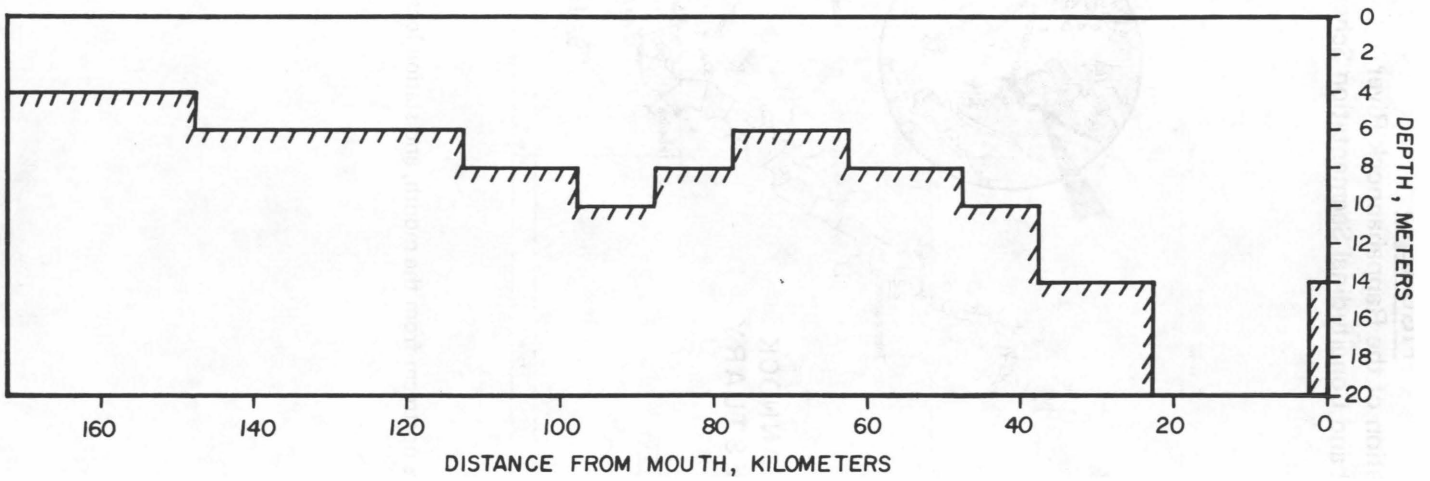

FIGURE 15

Comparison Between the Computed Tidal Range and the Range Tabulated in the Tide Tables (River Flow = 23 m^3/sec)

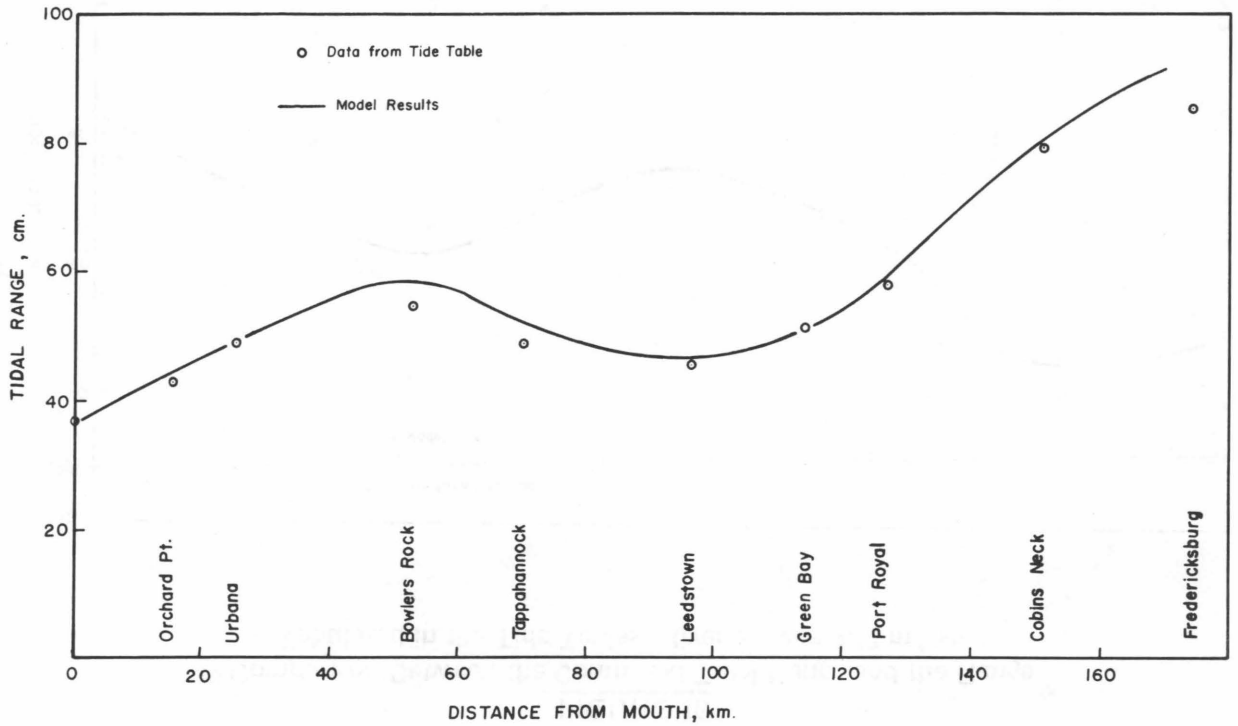

FIGURE 16

Comparison Between the Computed Tidal Range and the Range Tabulated in the Tide Tables (River Flow = 122 m^3/sec)

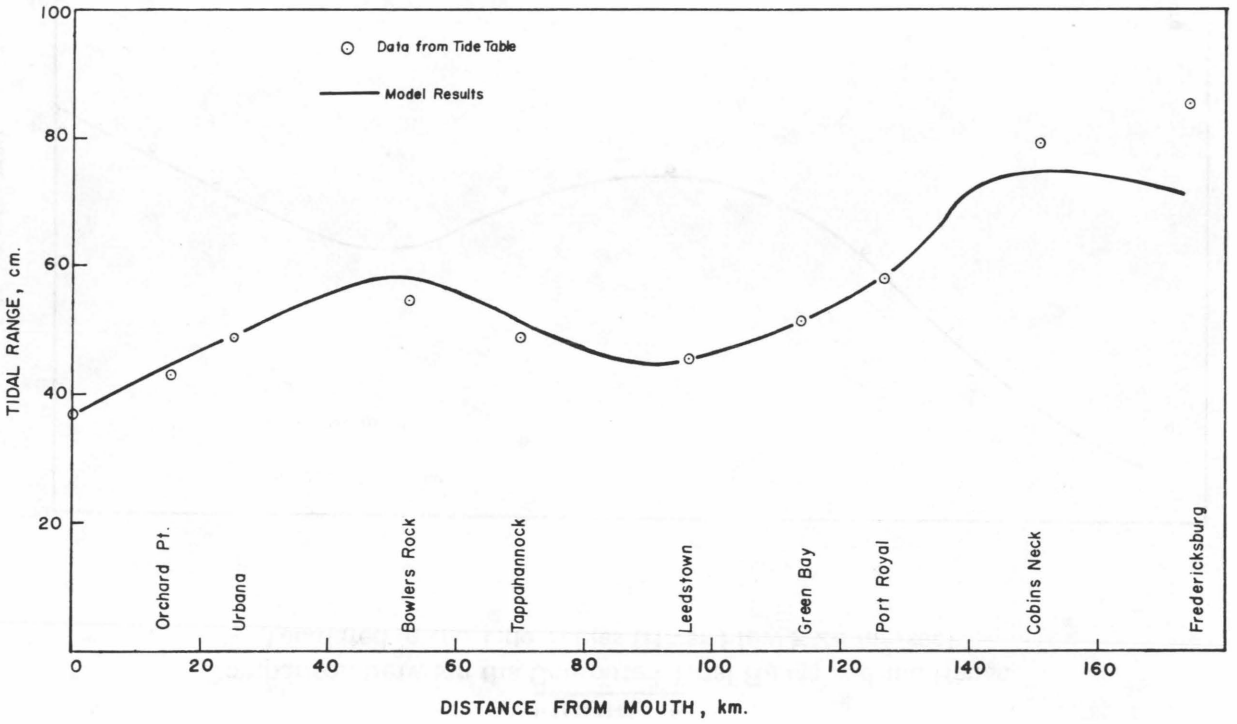

FIGURE 17

Comparison Between the Computed Tidal Phase and the Phase Tabulated in the Tide Tables (River Flow = 23 m^3/sec)

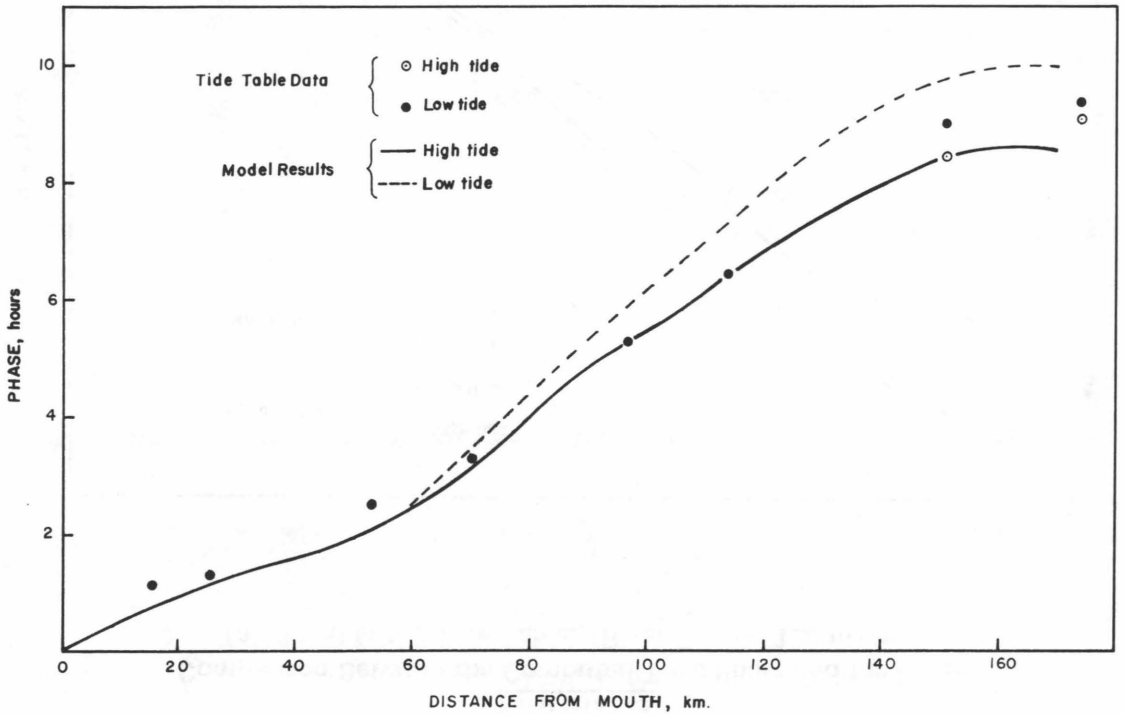

FIGURE 18

Comparison Between the Computed Tidal Phase and the Phase Tabulated in the Tide Tables (River Flow = 122 m^3/sec)

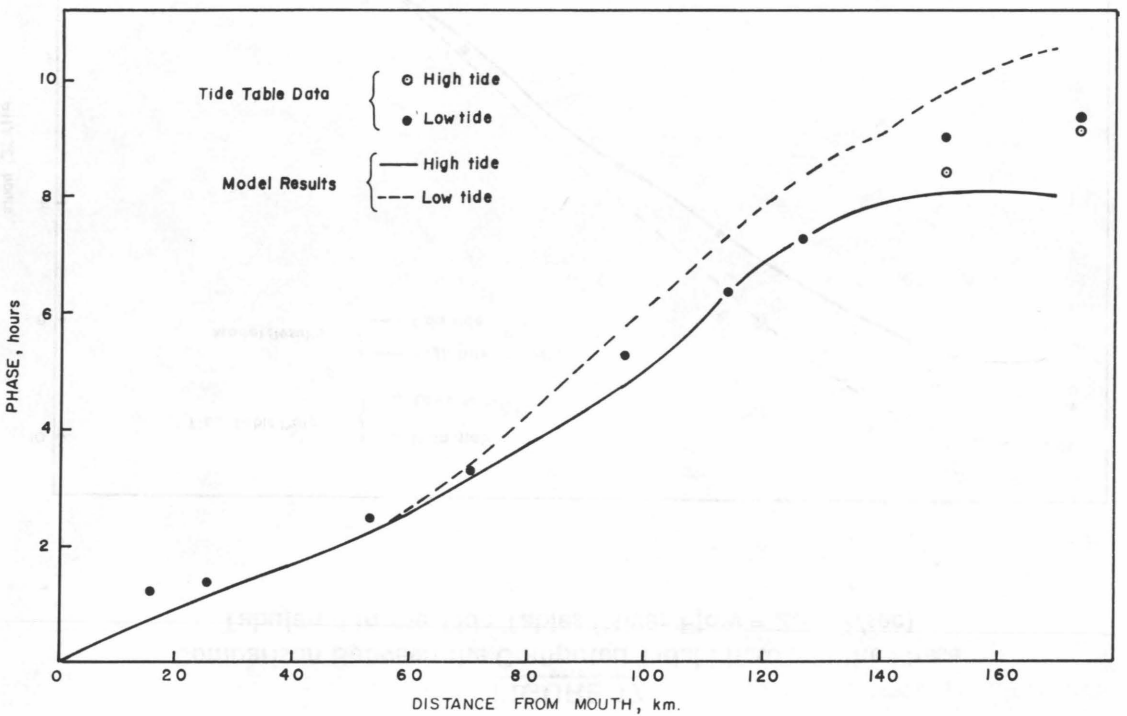

FIGURE 19

Comparison of Tidal Stage and Tidal Current at Various Stations (River Flow = 23 m^3/sec)*

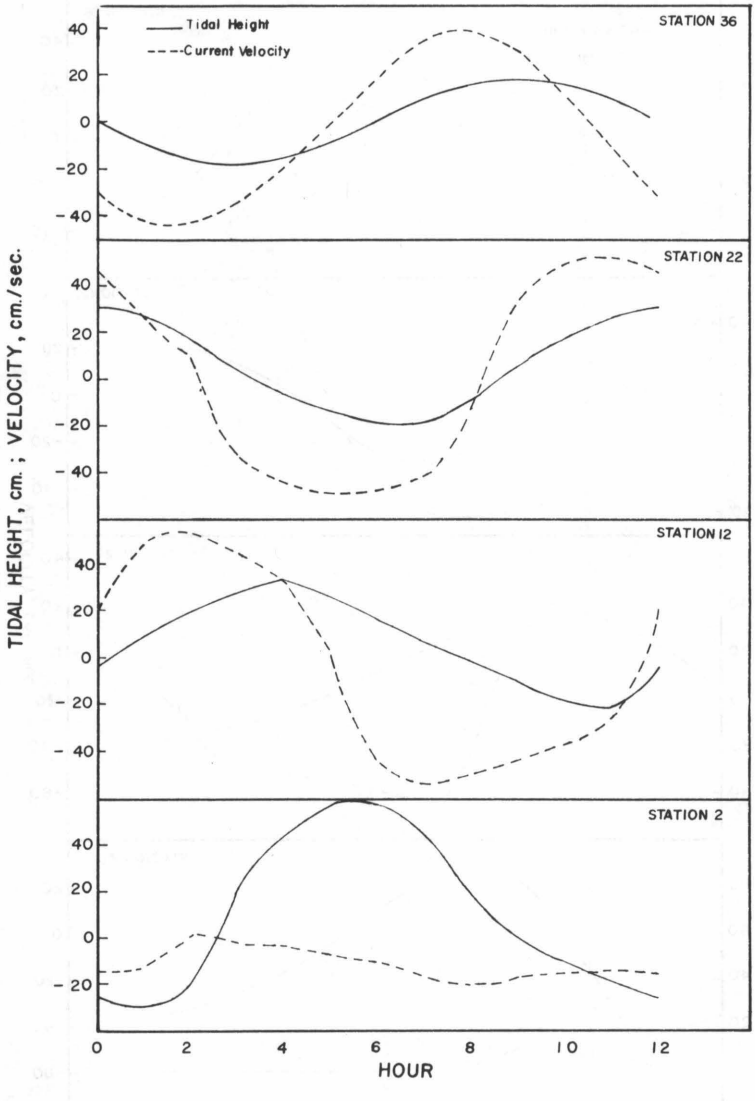

*For station 2, the actual current presented is that of station 3.

FIGURE 20

Comparisons of Tidal Stage and Tidal Current at Various Stations (River Flow = 122 m^3/sec)*

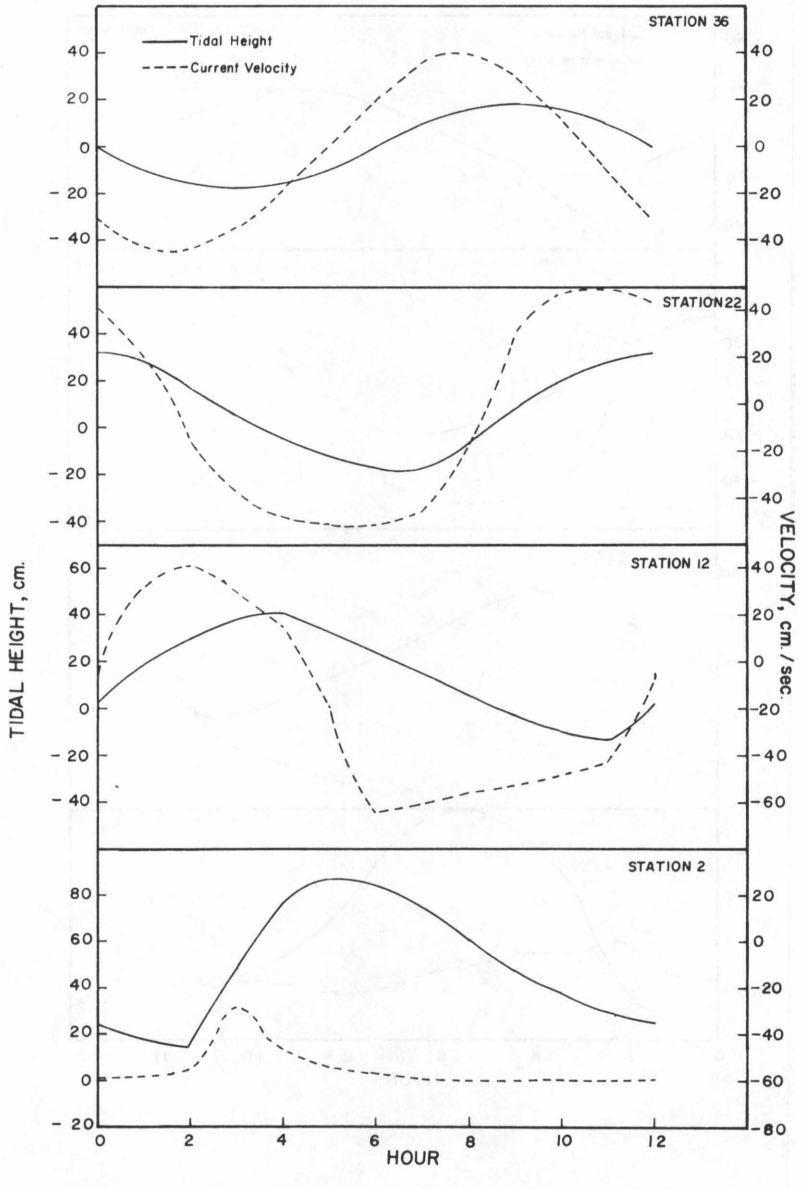

*For station 2, the actual current presented is that of station 3.

FIGURE 21
Tidally Averaged Salinity and Velocity Distributions
(River Flow = 122 m^3/sec in the Model)

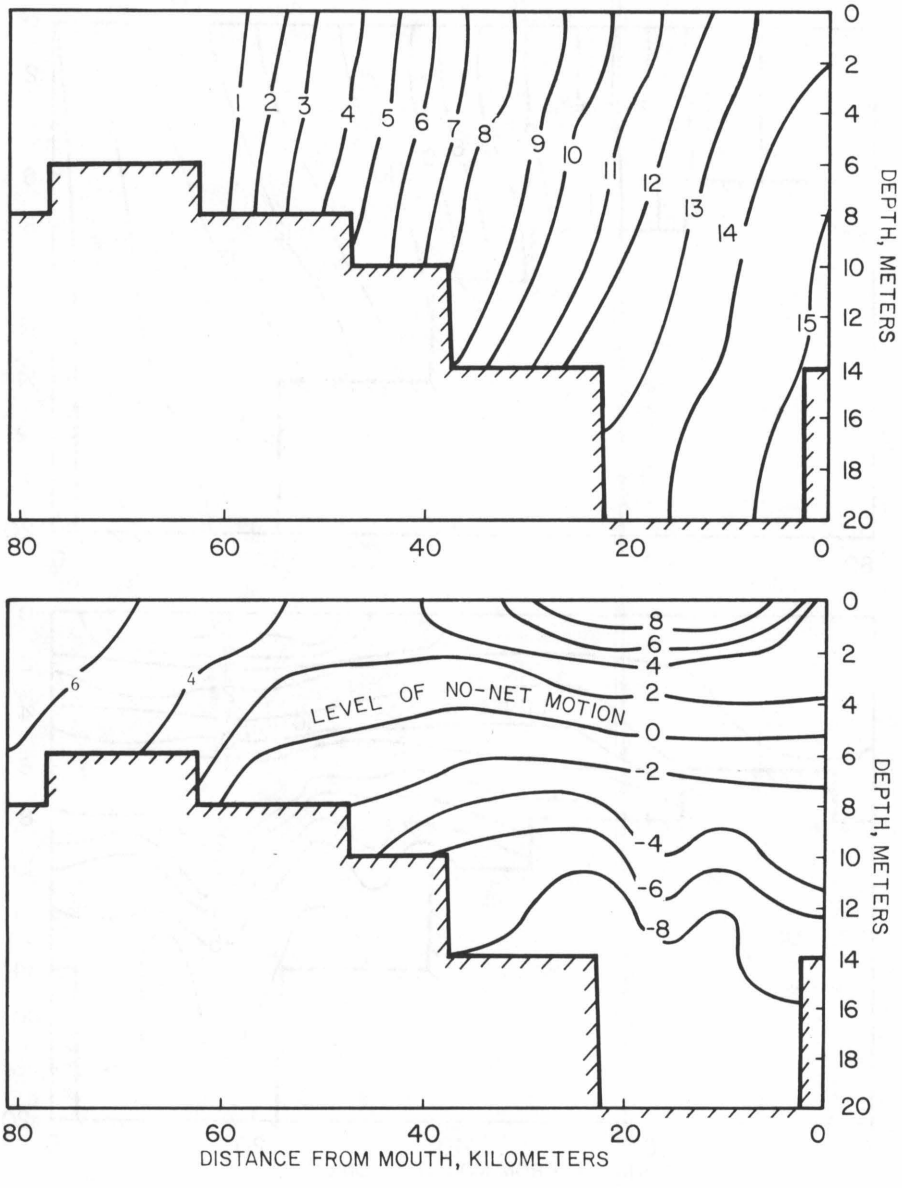

FIGURE 22

Tidally Averaged Salinity and Velocity Distributions
(River Flow = 23m^3/sec in the Model)

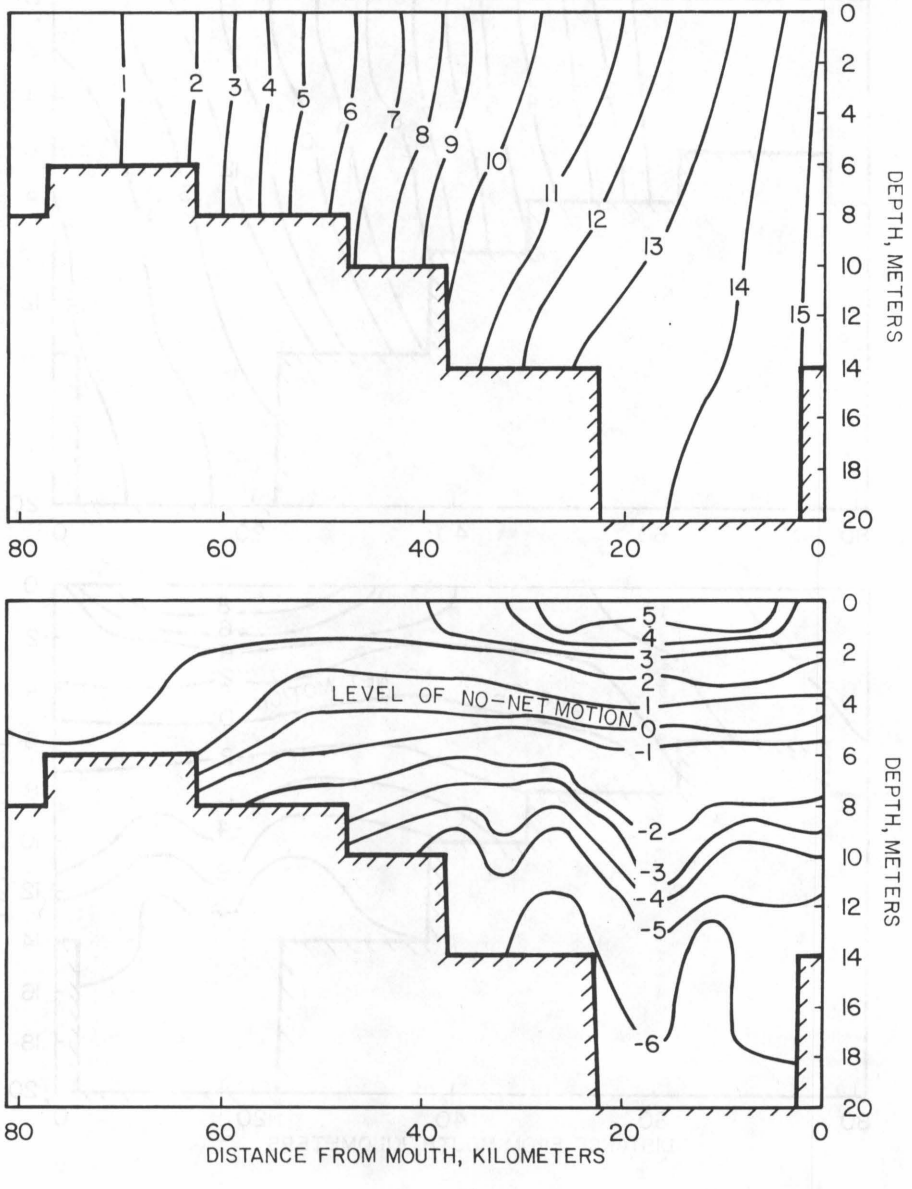

FIGURE 23

Tidally Averaged Suspended Sediment Distributions in the Model

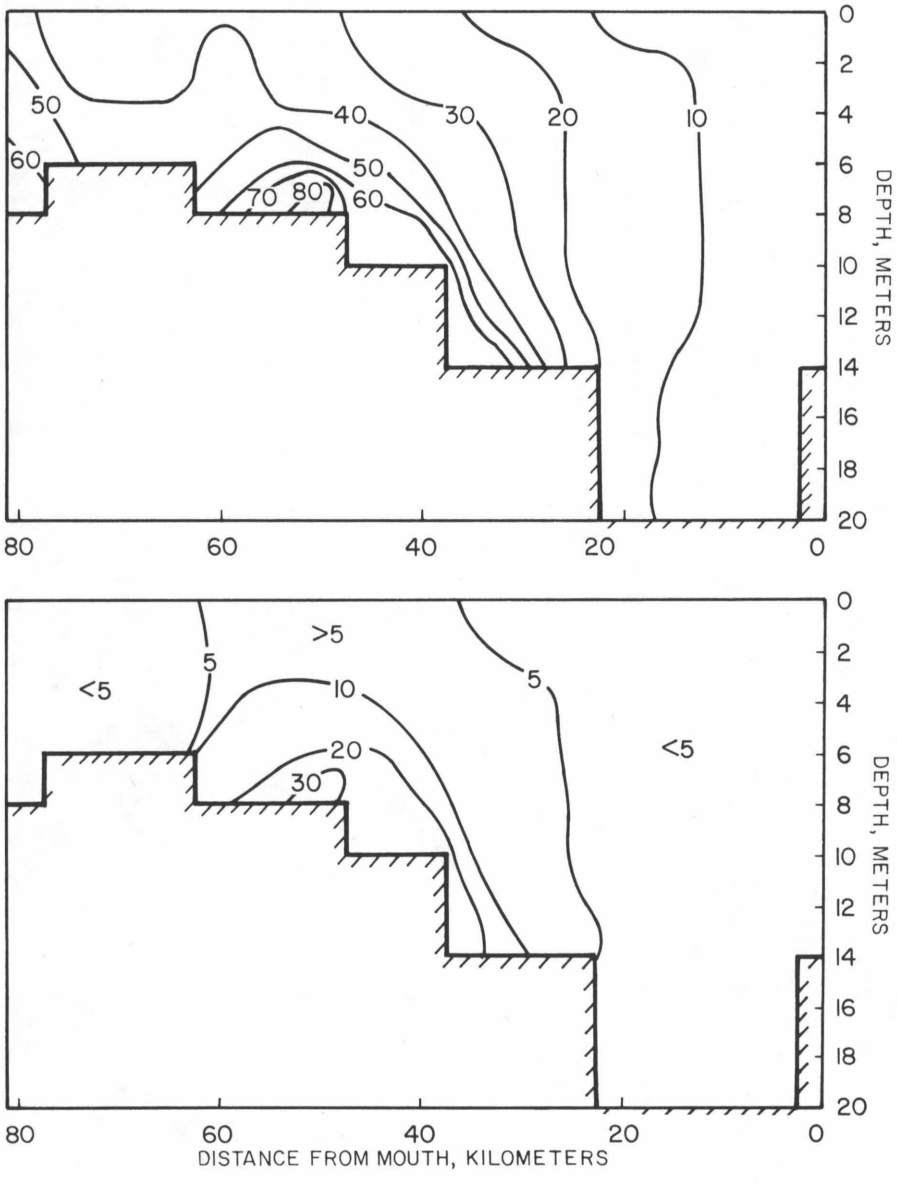

APPENDIX
Finite Difference Equations

I. Expansion of Equations

Equations 23, 24, 25, 26, and 27 are finite difference equations using the notations of Shuman [1962]. The compact notations are convenient for derivation and presentation. The following are the details of finite difference formulations which are actually used for computer programming.

The finite difference formulations for the terms in equation 23 are:

$$\overline{\delta_t}^{t}\eta = \frac{1}{2\Delta t}(\eta_{i,3} - \eta_{i,1})$$

$$w_1 \bar{B}_1^{z} = w_{i,1,2} \cdot \frac{1}{2}(B_{i,1} + B_{i,2})$$

$$\delta_x(u\bar{B}^{x}\bar{h}^{x})_1 = \frac{1}{\Delta x}\{u_{i+1,1,2} \cdot \frac{1}{2}(B_{i,1} + B_{i+1,1})$$

$$(h_1 + \frac{\eta_{i,2} + \eta_{i+1,2}}{2})$$

$$- \; u_{i,1,2} \cdot \frac{1}{2}(B_{i-1,1} + B_{i,1})$$

$$(h_1 + \frac{\eta_{i-1,2} + \eta_{i,2}}{2})\}$$

Therefore, equation 23 becomes:

$$\eta_{i,3} = \eta_{i,1} + \frac{\Delta t}{B_1}(B_{i,1} + B_{i,2}) \cdot w_{i,1,2}$$

$$- \frac{\Delta t}{B_1 \cdot \Delta x}\{u_{i+1,1,2}(B_{i,1} + B_{i+1,1})(h_1 + \frac{\eta_{i,2} + \eta_{i+1,2}}{2})$$

$$- u_{i,1,2}(B_{i-1,1} + B_{i,1})(h_1 + \frac{\eta_{i-1,2} + \eta_{i,2}}{2})\}$$

$$+ 2\Delta t \cdot q_1(h_1 + \eta_{i,2})/B_1$$

The terms in equation 24 are:

$$h\,\delta_z(\bar{B}^z w) = \frac{1}{2}(B_{i,k-1} + B_{i,k})\,w_{i,k-1,3} - \frac{1}{2}(B_{i,k} + B_{i,k+1})w_{i,k,3}$$

$$\delta_x(u\bar{B}^x\bar{h}^x) = \frac{1}{\Delta x}\{u_{i+1,k,3}\cdot\frac{1}{2}(B_{i,k}+B_{i+1,k})h_k - u_{i,k,3}\cdot\frac{1}{2}(B_{i-1,k}+B_{i,k})h_k\}$$

and equation 24 becomes:

$$w_{i,k-1,3} = \frac{1}{B_{i,k-1}+B_{i,k}}\Big[(B_{i,k}+B_{i,k+1})w_{i,k,3} - \frac{1}{\Delta x}\{u_{i+1,k,3}(B_{i,k}+B_{i+1,k})h_k - u_{i,k,3}(B_{i-1,k}+B_{i,k})h_k\} + 2q_k h_k\Big)$$

The finite difference formulations for the terms in equation 25 are:

$$\overline{\delta_t(u\bar{h}^x\bar{B}^x)}^t = \frac{1}{2\Delta t}\cdot\frac{B_{i-1,k}+B_{i,k}}{2}\{u_{i,k,3}(h_k+\alpha\cdot\frac{\eta_{i-1,3}+\eta_{i,3}}{2}) - u_{i,k,1}(h_k+\alpha\cdot\frac{\eta_{i-1,1}+\eta_{i,1}}{2})\}$$

where $\alpha = 1$ for the surface layer and $\alpha = 0$ for the remaining layers:

$$\overline{\delta_x(\bar{B}^x\bar{h}^x u\,\bar{u}^x)}^x = \frac{1}{\Delta x}\Big(\frac{1}{2}\{\frac{B_{i-1,k}+B_{i,k}}{2}(h_k+\alpha\cdot\frac{\eta_{i-1,2}+\eta_{i,2}}{2})u_{i,k,2} + \frac{B_{i,k}+B_{i+1,k}}{2}(h_k+\alpha\cdot\frac{\eta_{i,2}+\eta_{i+1,2}}{2})u_{i+1,k,2}\}\cdot\frac{1}{2}(u_{i,k,2}+u_{i+1,k,2}) - \frac{1}{2}\{\frac{B_{i-2,k}+B_{i-1,k}}{2}(h_k+\alpha\cdot\frac{\eta_{i-2,2}+\eta_{i-1,2}}{2})u_{i-k,k,2}$$

$$+ \frac{B_{i-1,k} + B_{i,k}}{2} (h_k + \alpha \cdot \frac{\eta_{i-1,2} + \eta_{i,2}}{2}) u_{i,k,2} \}$$

$$\cdot \frac{1}{2} (u_{i-1,k,2} + u_{i,k,2}))$$

$$\bar{h}^z \delta_z (\bar{u}^z \bar{w}^x \bar{B}^{xz}) = \frac{1}{2} (u_{i,k-1,2} + u_{i,k,2}) \cdot \frac{1}{2} (w_{i-1,k-1,2} + w_{i,k-1,2})$$

$$\frac{1}{4} (B_{i-1,k-1} + B_{i-1,k} + B_{i,k-1} + B_{i,k})$$

$$- \frac{1}{2} (u_{i,k,2} + u_{i,k+1,2}) \cdot \frac{1}{2} (w_{i-1,k,2} + w_{i,k,2})$$

$$\frac{1}{4} (B_{i-1,k} + B_{i-1,k+1} + B_{i,k} + B_{i,k+1})$$

$$\frac{\bar{B}^x \bar{h}^x}{\bar{\rho}^x} (\frac{\partial P}{\partial x})_k = (B_{i-1,k} + B_{i,k}) (h_k + \alpha \cdot \frac{\eta_{i-1,2} + \eta_{i,2}}{2}) / (\rho_{i-1,k,2} +$$

$$\rho_{i,k,2}) \ (\frac{\partial P}{\partial x})_k$$

$$\delta_x (\overline{\bar{B}^x \bar{h}^x e_x}^x \ \delta_x u)_- =$$

$$\frac{1}{\Delta x} \Big(\frac{1}{2} \{ \frac{1}{2} (B_{i-1,k} + B_{i,k}) (h_k + \alpha \cdot \frac{\eta_{i-1,1} + \eta_{i,1}}{2}) (e_x)_{i,k}$$

$$+ \frac{1}{2} (B_{i,k} + B_{i+1,k}) (h_k + \alpha \cdot \frac{\eta_{i,1} + \eta_{i+1,1}}{2}) (e_x)_{i+1,k} \}$$

$$(u_{i+1,k,1} - u_{i,k,1}) / \Delta x$$

$$- \frac{1}{2} \{ \frac{1}{2} (B_{i-2,k} + B_{i-1,k}) (h_k + \alpha \cdot \frac{\eta_{i-2,1} + \eta_{i-1,1}}{2} (e_x)_{i-1,k}$$

$$+ \frac{1}{2} (B_{i-1,k} + B_{i,k}) (h_k + \alpha \cdot \frac{\eta_{i-1,1} + \eta_{i,1}}{2}) (e_x)_{i,k} \}$$

$$(u_{i,k,1} - u_{i-1,k,1}) / \Delta x \Big)$$

$$\bar{h}^z \ \delta_z (\bar{e}_z^x \ \bar{B}^{xz} \ \delta_z u)_- =$$

$$\frac{1}{2} \{ (e_z)_{i-1,k-1} + (e_z)_{i,k-1} \} \cdot \frac{1}{4} (B_{i-1,k-1} + B_{i,k-1}$$

$$+ B_{i-1,k} + B_{i,k})(u_{i,k-1,1} - u_{i,k,1})/\tfrac{1}{2}(h_{k-1} + h_k)$$

$$- \tfrac{1}{2}\{(e_z)_{i-1,k} + (e_z)_{i,k}\} \cdot \tfrac{1}{4}(B_{i-1,k} + B_{i,k} + B_{i-1,k+1}$$

$$+ B_{i,k+1})(u_{i,k,1} - u_{i,k+1,1})/\tfrac{1}{2}(h_k + h_{k+1}) - \text{side friction}$$

where side friction = $k\, u_{i,k,1}|u_{i,k,1}| \cdot (B_{i-1,k} + B_{i,k}$

$$- B_{i-1,k+1} - B_{i,k+1})/2$$

Therefore, equation 25 becomes:

$$u_{i,k,3} = \frac{1}{h_k + \alpha \cdot \frac{\eta_{i-1,3} + \eta_{i,3}}{2}} \left[(h_k + \alpha \cdot \frac{\eta_{i-1,1} + \eta_{i,1}}{2}) u_{i,k,1}\right.$$

$$- \frac{\Delta t}{2\Delta x(B_{i-1,k} + B_{i,k})} \{(B_{i-1,k} + B_{i,k})(h_k +$$

$$\alpha \cdot \frac{\eta_{i-1,2} + \eta_{i,2}}{2}) u_{i,k,2} + (B_{i,k} + B_{i+1,k})(h_k +$$

$$\left.\alpha \cdot \frac{\eta_{i,2} + \eta_{i+1,2}}{2}) u_{i+1,k,2}\right\}(u_{i,k,2} + u_{i+1,k,2})$$

$$+ \frac{\Delta t}{2\Delta x(B_{i-1,k} + B_{i,k})} \{(B_{i-2,k} + B_{i-1,k})(h_k +$$

$$\alpha \cdot \frac{\eta_{i-2,2} + \eta_{i-1,2}}{2}) u_{i-1,k,2} + (B_{i-1,k} + B_{i,k})(h_k +$$

$$\alpha \cdot \frac{\eta_{i-1,2} + \eta_{i,2}}{2}) u_{i,k,2}\}(u_{i-1,k,2} + u_{i,k,2})$$

$$- \frac{\Delta t}{4(B_{i-1,k} + B_{i,k})} \{(u_{i,k-1,2} + u_{i,k,2})(w_{i-1,k-1,2} +$$

$$w_{i,k-1,2})(B_{i-1,k-1} + B_{i-1,k} + B_{i,k-1} + B_{i,k})$$

$$-(u_{i,k,2} + u_{i,k+1,2})(w_{i-1,k,2} + w_{i,k,2})$$

$$(B_{i-1,k} + B_{i-1,k+1} + B_{i,k} + B_{i,k+1})$$

$$- 4\cdot\Delta t(h_k + \alpha\cdot\frac{\eta_{i-1,2} + \eta_{i,2}}{2})(\frac{\partial P}{\partial x})_k/(\rho_{i-1,k,2} + \rho_{i,k,2})$$

$$+ \frac{\Delta t}{(\Delta x)^2(B_{i-1,k} + B_{i,k})}\{(B_{i-1,k} + B_{i,k})(h_k +$$

$$\alpha\cdot\frac{\eta_{i-1,1} + \eta_{i,1}}{2})(e_x)_{i,k} + (B_{i,k} + B_{i+1,k})(h_k +$$

$$\alpha\cdot\frac{\eta_{i,1} + \eta_{i+1,1}}{2})(e_x)_{i+1,k}\}(u_{i+1,k,1} - u_{i,k,1})$$

$$- \frac{\Delta t}{(\Delta x)^2(B_{i-1,k} + B_{i,k})}\{(B_{i-2,k} + B_{i-1,k})(h_k +$$

$$\alpha\cdot\frac{\eta_{i-2,1} + \eta_{i-1,1}}{2})(e_x)_{i-1,k} + (B_{i-1,k} + B_{i,k})(h_k +$$

$$\alpha\cdot\frac{\eta_{i-1,1} + \eta_{i,1}}{2})(e_x)_{i,k}\}(u_{i,k,1} - u_{i-1,k,1})$$

$$+ \frac{\Delta t}{B_{i-1,k} + B_{i,k}}\{(e_z)_{i-1,k-1} + (e_z)_{i,k-1}\}(B_{i-1,k-1} +$$

$$B_{i,k-1} + B_{i-1,k} + B_{i,k})(u_{i,k-1,1} - u_{i,k,1})/(h_{k-1} + h_k)$$

$$- \frac{\Delta t}{B_{i-1,k} + B_{i,k}}\{(e_z)_{i-1,k} + (e_z)_{i,k}\}(B_{i-1,k} +$$

$$B_{i,k} + B_{i-1,k+1} + B_{i,k+1})(u_{i,k,1} - u_{i,k+1,1})/(h_k + h_{k+1})$$

$$+ \frac{4\Delta t}{B_{i-1,k} + B_{i,k}}\cdot q_{i,k}\cdot u_t\cdot h_k) - \text{side friction}$$

The finite difference formulation for terms in equation 26 are:

$$\overline{\delta_t(shB)}^t = \frac{B_{i,k}}{2\Delta t}\{s_{i,k,3}(h_k + \alpha\cdot\eta_{i,3}) - s_{i,k,1}(h_k + \alpha\cdot\eta_{i,1})\}$$

where $\alpha = 1$ for the surface layer and $\alpha = 0$ for the remaining layers:

$$\delta_x(\bar{B}^x\bar{h}^x\bar{s}^x u) = \frac{1}{\Delta x}\{\frac{1}{2}(B_{i,k} + B_{i+1,k})\cdot(h_k + \alpha\cdot\frac{\eta_{i,2} + \eta_{i+1,2}}{2})\cdot$$

$$\frac{1}{2}(s_{i,k,2} + s_{i+1,k,2})\ u_{i+1,k,2}$$

$$- \frac{1}{2}(B_{i-1,k} + B_{i,k})(h_k + \alpha\cdot\frac{\eta_{i-1,2} + \eta_{i,2}}{2})$$

$$\frac{1}{2}(s_{i-1,k,2} + s_{i,k,2})\ u_{i,k,2}\}$$

$$h\ \delta_z(w\ \bar{s}^z\bar{B}^z) = w_{i,k-1,2}\cdot\frac{1}{2}(s_{i,k-1,2} + s_{i,k,2})\cdot\frac{1}{2}(B_{i,k-1} +$$

$$B_{i,k}) - w_{i,k,2}\cdot\frac{1}{2}(s_{i,k,2} + s_{i,k+1,2})\cdot\frac{1}{2}(B_{i,k} + B_{i,k+1})$$

$$\delta_x(E_x\bar{B}^x\bar{h}^x\delta_x s)_- = \frac{1}{\Delta x}\{(E_x)_{i+1,k,1}\cdot\frac{1}{2}(B_{i,k} + B_{i+1,k})\cdot$$

$$(h_k + \alpha\cdot\frac{\eta_{i,1} + \eta_{i+1,1}}{2})\cdot\frac{1}{\Delta x}(s_{i+1,k,1} - s_{i,k,1})$$

$$- (E_x)_{i,k,1}\cdot\frac{1}{2}(B_{i-1,k} + B_{i,k})\cdot$$

$$(h_k + \alpha\cdot\frac{\eta_{i-1,1} + \eta_{i,1}}{2})\cdot\frac{1}{\Delta x}(s_{i,k,1} - s_{i-1,k,1})\}$$

$$h\ \delta_z(E_z\ \bar{B}^z\delta_z\ s)_- = (E_z)_{i,k-1,1}\cdot\frac{1}{2}(B_{i,k-1} + B_{i,k})\cdot$$

$$\frac{2}{h_{k-1} + h_k}(s_{i,k-1,1} - s_{i,k,1}) - (E_z)_{i,k}\cdot\frac{1}{2}(B_{i,k} +$$

$$B_{i,k+1})\cdot\frac{2}{h_k + h_{k+1}}(s_{i,k,1} - s_{i,k+1,1})$$

Therefore, equation 26 becomes:

$$s_{i,k,3} = \frac{1}{h_k + \alpha\eta_{1,3}}\{(h_k + \alpha\eta_{i,1})\ s_{i,k,1} - \frac{\Delta t}{B_{i,k}\cdot\Delta x}\{(B_{i,k} +$$

$$B_{i+1,k}) \cdot (h_k + \alpha \cdot \frac{\eta_{i,2} + \eta_{i+1,2}}{2}) \cdot$$

$$\frac{1}{2} (s_{i,k,2} + s_{i+1,k,2}) u_{i+1,k,2} - (B_{i-1,k} +$$

$$B_{i,k})(h_k + \alpha \cdot \frac{\eta_{i-1,2} + \eta_{i,2}}{2}) \cdot \frac{1}{2} (s_{i-1,k,2} + s_{i,k,2})$$

$$u_{i,k,2}\} - \frac{\Delta t}{B_{i,k}}\{w_{i,k-1,2}(s_{i,k-1,2} + s_{i,k,2}) \cdot$$

$$\frac{1}{2} (B_{i,k-1} + B_{i,k}) - w_{i,k,2}(s_{i,k,2} + s_{i,k+1,2}) \cdot$$

$$\frac{1}{2} (B_{i,k} + B_{i+1,k}) + \frac{\Delta t}{B_{i,k} \cdot \Delta x}\{(F_x)_{i+1,k,1}(B_{i,k} +$$

$$B_{i+1,k})(h_k + \alpha \cdot \frac{\eta_{i,1} + \eta_{i+1,1}}{2}) \cdot \frac{1}{\Delta x}(s_{i+1,k,1} - s_{i,k,1}) -$$

$$(E_x)_{i,k,1} (B_{i-1,k} + B_{i,k})(h_k + \alpha \cdot \frac{\eta_{i-1,1} + \eta_{i,1}}{2}) \cdot$$

$$\frac{1}{\Delta x}(s_{i,k,1} - s_{i-1,k,1})\} + \frac{\Delta t}{B_{i,k}}\{(E_z)_{i,k-1,1}(B_{i,k-1} +$$

$$B_{i,k}) \cdot \frac{2}{h_{k-1} + h_k}(s_{i,k-1,1} - s_{i,k,1}) -$$

$$(E_z)_{i,k} (B_{i,k} + B_{i,k+1}) \cdot \frac{2}{h_{k-1} + h_{k+1}}(s_{i,k,1} -$$

$$s_{i,k+1,1})\} + \frac{2\Delta t}{B_{i,k}} \cdot q \cdot s_t \cdot h_k)$$

Equations 27 and 26 are identical except for the additional terms involving the settling velocity, resuspension, and deposition of sediment particles. The mathematical formulations of these terms have been discussed in detail in the main text.

II. Treatment of Embayment as Storage Area

The two-dimensional model considers the longitudinal and vertical variations of dependent variables along the conveying channel of the estuary. In segments where there is substantial area of embayment, the water particle momentum and sediment concentration in the embayment will be quite different from those in the conveying channel. While the model cannot calculate this variation, it shall account for the exchange of mass and momentum between the channel and embayment.

Let $SST(I)$ be the surface area of the embayment in the Ith segment; the equivalent width of the storage area may be defined as:

$$STB(I) = SST(I)/\Delta x$$

where Δx is the distance between grid points. Since only the time variations of mass and momentum in the storage area will affect the main channel, the exchange of mass and momentum may be assumed to happen only at top layer, where the surface elevation of the storage area rises and falls with that of the conveying channel.

For the mass exchange of water, it is required that the width of the top layer $B(I, 1)$ in the denominator of continuity equation (equation 23) be changed to $B(I, 1) + STB(I)$. For the mass exchange of a dissolved substance, e.g., sea salt, a sink (or source) term is needed, to be added to the right hand side of equation 26.

$$\text{sink term} = - s_{i,k,2} \cdot STB(I)(\eta_{i,3} - \eta_{i,1})/2\Delta t$$

For the momentum exchange, it may be assumed that the conveying channel will lose all the momentum of the water particles entering into storage area and receive no momentum from the water particles coming from storage area. Therefore, a sink term is needed, to be added to the right hand side of momentum equation (equation 25):

$$\text{sink term} = -u_{i,k,2} \cdot \frac{1}{2}\,(STB(I-1) + STB(I)) \cdot \frac{1}{2}\,(\eta_{i-1,3}^{+} \eta_{i,3}^{-} \eta_{i-1,1}^{-} \eta_{i,1})/\Delta t$$

$$\text{if } \eta_{i-1,3}^{+} \eta_{i,3}^{-} \eta_{i-1,1}^{-} \eta_{i,1} > 0$$

sink term = 0 otherwise.

The Virginia Water Resources Research Center is a federal-state partnership agency attempting to find solutions to the state's water resource problems through careful research and analysis. Established at Virginia Polytechnic Institute and State University under provisions of the Water Resources Research Act of 1964 (P.L. 88-379), the Center serves five primary functions:

- It studies the state's water and related land-use problems, including their ecological, political, economic, institutional, legal, and social implications.
- It sponsors and administers research investigations of these problems.
- It collects and disseminates information about water resources and water resources research.
- It provides training opportunities in research for future water scientists enrolled at the state's colleges and universities.
- It provides other public services to the state in a wide variety of forms.

More information on programs and activities may be obtained by contacting the Center at the address below.

Virginia Water Resources Research Center
617 North Main Street
Blacksburg, Virginia 24060
Phone (703) 951-5624